

This discussion paper is/has been under review for the journal *Climate of the Past* (CP).  
Please refer to the corresponding final paper in CP if available.

# Volcanic ash layers in Lake El'gygytgyn: eight new regionally significant chronostratigraphic markers for western Beringia

C. van den Bogaard<sup>1</sup>, B. J. L. Jensen<sup>2,\*</sup>, N. J. G. Pearce<sup>3</sup>, D. G. Froese<sup>2</sup>,  
M. V. Portnyagin<sup>1</sup>, V. V. Ponomareva<sup>4</sup>, D. Garbe-Schönberg<sup>5</sup>, and V. Wennrich<sup>6</sup>

<sup>1</sup>GEOMAR Helmholtz-Zentrum für Ozeanforschung Kiel, Wischhofstr. 1–3,  
24148 Kiel, Germany

<sup>2</sup>Department of Earth and Atmospheric Sciences, 1–26 Earth Sciences Building,  
University of Alberta, Edmonton, AB, T6G 2E3, Canada

<sup>3</sup>Department of Geography and Earth Sciences, Aberystwyth University, Llandinam Building,  
Penglais Campus, Aberystwyth, SY23 3DB, Wales, UK

<sup>4</sup>Institute of Volcanology and Seismology, Petropavlovsk-Kamchatsky, Russia

<sup>5</sup>Institute of Geoscience, Christian-Albrechts-University of Kiel, Kiel, Germany

<sup>6</sup>University of Cologne, Institute for Geology and Mineralogy, Cologne, Germany

\* now at: School of Geography, Archaeology and Palaeoecology,  
Queen's University Belfast, UK

5977

Received: 10 August 2013 – Accepted: 29 September 2013 – Published: 29 October 2013

Correspondence to: C. van den Bogaard (cbogaard@geomar.de)

Published by Copernicus Publications on behalf of the European Geosciences Union.

5978

## Abstract

Ash layers from explosive volcanic eruptions (i.e. tephra) represent isochronous surfaces independent from the environment in which they are deposited and the distance from their source. In comparison to eastern Beringia (non-glaciated Yukon and Alaska), few Plio-Pleistocene distal tephra are known from western Beringia (non-glaciated arctic and subarctic eastern Russia), hindering the dating and correlation of sediments beyond the limit of radiocarbon and luminescence methods. The identification of eight visible tephra layers (T0–T7) in sediment cores extracted from Lake El'gygytgyn, in the Far East Russian Arctic, indicates the feasibility of developing a tephrostratigraphic framework for this region. These tephra range in age from ca. 45 ka to 2.2 Ma, and each is described and characterized by its major-, minor-, trace-element and Pb isotope composition. These data show that subduction zone related volcanism from the Kurile–Kamchatka–Aleutian–Arc and Alaska Peninsula is the most likely source, with Pb isotope data indicating a Kamchatkan volcanic source for tephra layers T0–T5 and T7, while a source in the Aleutian Arc is possible probable for Tephra T6. The location of Lake El'gygytgyn relative to potential source volcanoes (> 1000 km) suggests these tephra are distributed over a vast area. These deposits provide a unique opportunity to correlate the high-resolution paleoenvironmental records of Lake El'gygytgyn to other terrestrial paleoenvironmental archives from western Beringia and marine records from the northwest Pacific and Bering Sea. This is an important first step towards the development of a robust integrated framework between the continuous paleoclimatic records of Lake El'gygytgyn and other terrestrial and marine records in NE Eurasia.

5979

## 1 Introduction

### 1.1 Lake drilling program and resultant cores

Lake El'gygytgyn is located in the Far East Russian Arctic (67°30' N, 172°5' E), 100 km north of the Arctic Circle (Fig. 1). The 12 km wide and 175 m deep lake formed within a meteorite impact crater created 3.58 ± 0.04 million yr ago (Gurov et al., 1978, 2007; Layer, 2000), and was cored under a jointly-funded project led by the Inter-Continental Drilling Program (ICDP) in winter 2008/2009. Two pilot cores (LZ 1024, PG1351) were collected from Lake El'gygytgyn during initial pre-site surveys (Juschus et al., 2009), followed by the main drilling program that collected three cores from the center of the lake (ICDP site 5011; holes 5011-1A, 5011-1B, 5011-1C; 67°29.98' N, 172°6.23' E), and one permafrost core at the lake margin (ICDP site 5011-3A; 76°29.1' N, 171°56.7' E) (Melles et al., 2011, 2012). Approximately 315 m of lacustrine sediment were cored without hiatuses, spanning the uppermost Pliocene to present (Melles et al., 2011, 2012). Tephra layers were identified and collected from all five lake cores, and were initially correlated by stratigraphy and assigned numerically based names, T0–T7.

### 1.2 Background

Tephra resulting from explosive volcanic eruptions can be distributed over vast areas. Because an eruption occurs over days to weeks, each tephra layer represents an isochronous horizon in the different types of depositional environments in which it is preserved. Each tephra potentially has a unique geochemical fingerprint, allowing correlation of the archives it is present within, and some can be independently dated (e.g. Shane et al., 1996; Westgate et al., 2001; Giaccio et al., 2012). The value of tephra layers has become increasingly recognized in climate and environmental studies over the last few decades. Tephra have been recovered from soil records, loess deposits, lake sediments, peat bogs, archaeological sites, marine and ice cores. As cryptotephra layers – a volcanic ash layer not visible to the naked eye – they have been traced as far

5980

as 7000 km from their source (e.g. Dugmore et al., 1989; Grönvold et al., 1995; Pilcher et al., 1996; van den Bogaard and Schmincke, 2002; Davies et al., 2003; Wastegård, 2002; Davies et al., 2012; Dörfler et al., 2012; Jensen et al., 2012; Pyne-O'Donnell et al., 2012; Lane et al., 2013).

5 The tephra beds present in Lake El'gygytgyn are of particular interest because of its location within western Beringia (Brigham-Grette et al., 2007). Western Beringia is the Eurasian half of Beringia, a large region extending from eastern Siberia to far northwestern Canada that was never glaciated (e.g. Hultén, 1937; Hopkins, 1967; Schirmermeister et al., 2013). The lack of glaciation and presence of permafrost has resulted in exceptionally well-preserved paleoenvironmental archives that go well beyond the last glacial-interglacial cycle (e.g. Westgate et al., 1990; Sher, 1997; Froese et al., 2009; Minyuk and Ivanov, 2012). In eastern Beringia (Yukon and Alaska), abundant volcanic ash from the Aleutian Arc–Alaska Peninsula and Wrangell volcanic field have been instrumental in providing a means to date and correlate these archives back approximately 2.5 Ma (e.g. Preece et al., 1999, 2011a, b; Jensen et al., 2008, 2011, 2013; Reyes et al., 2010). However, because few tephra have ever been recognized in western Beringian sediments, and the idea that prevailing wind directions tend to keep tephra “out of reach” of this region, little work has been done to examine the exposures for their presence. This has had a significant impact on attempting to identify sediments that are beyond the limits of radiocarbon and luminescence dating (e.g. Sher, 1991).

20 Lake El'gygytgyn sediment cores contain a minimum of eight visible tephra layers that are up to several cm thick. The closest known volcanic field to Lake El'gygytgyn is more than 300 km away, and volcanoes with known explosive eruptions that have been active during the Late Neogene are  $\geq 1000$  km away in the Kurile–Kamchatka–Aleutian–Arc and Alaska Peninsula (Fig. 1). This implies that this lake holds a record of distant very large magnitude eruptions, which must be distributed widely over western Beringia. In fact, initial analyses of the “T1 tephra” from the pilot core LZ 1024 indicate that it correlates to the Rauchua tephra, thought to be Kamchatka-sourced and present at coastal bluffs on the East Siberian Sea, as well as in the Bering Sea

5981

(SO201-2-81KL) and northwest Pacific (SO201-2-40KL) marine cores (Ponomareva et al., 2013b). The correlation of T1 to the Rauchua tephra, a tephra only  $\sim 1$  cm thick in the Lake El'gygytgyn cores, suggests that each individual layer (several  $> 1$  cm thick) has the potential to play an important role in correlating and dating the disparate paleoenvironmental records of this region.

5 With this study our goal is to provide a detailed geochemical fingerprint for each individual tephra layer in the Lake El'gygytgyn cores. These data support the stratigraphic correlations that have been made between the five lake cores, and enable us to identify the most likely source regions. The geochemical fingerprints, comprising major-, minor- and trace-element geochemistry and lead (Pb) isotopes, will allow for the future identification of these tephra beds in other depositional settings where they have been preserved, providing important new chronostratigraphic markers for western Beringia. These tephra will also provide an independent correlation tool for the Lake El'gygytgyn climate records, particularly to the marine records from Bering Sea and northwest Pacific. This should provide a means to compare age models, and allow inter-regional comparisons with sufficiently high temporal precision to discuss climatic synchronicity.

## 2 Summary of analytical methods



20 All visible tephra layers identified in the cores were sampled and investigated petrologically prior to analysis by electron probe microanalysis (EPMA) and laser ablation inductively coupled plasma-mass spectrometry (LA-ICP-MS) for compositional fingerprinting, whereby the major-, minor-, trace-element and Pb isotopic composition of single volcanic glass shards was determined. Major and minor-element geochemistry was determined via wave-length dispersive EPMA at the University of Alberta, Edmonton (e.g. Jensen et al., 2008, 2011) and at GEOMAR, Kiel (e.g. Ponomareva et al., 2013). Both laboratories contributed to the recent INTAV (International Quaternary Association's focus group on tephrochronology) comparison of tephrochronology laboratories, which confirmed the high quality of the major-element data produced by both

5982

instruments (Kuehn et al., 2011). Additionally, both laboratories run the Lipari obsidian standard ID 3506 as a secondary glass standard to track the quality of calibration throughout each run (Kuehn et al., 2011). Therefore, both instruments produce data sets that are identical within statistical deviations, and the secondary standard data  
5 allows direct comparison of the data sets and helps correct for potential issues arising from inter-laboratory calibration differences.

Trace element analyses were performed by LA-ICP-MS at Aberystwyth University on the glass component of individual shards using ablation craters with diameters in the range of 10–20 µm. Most analyses were carried out on the same sample mounts used  
10 for the majority of the EPMA. Detailed methods are described in Pearce et al. (2011); NIST 612 was used for calibration (Pearce et al., 1997), and <sup>29</sup>Si as the internal standard, using concentrations determined by EPMA. After rejection of analyses for the incorporation of phenocrysts and/or microlites (e.g. using elevated Ca or Sr for the presence of feldspar) into the ablated material (see analytical protocols established in  
15 Pearce et al., 2002, 2004a, 2007), a total of 226 individual shards were analysed from the eight tephra units in Lake El'gygytgyn. Trace element analyses of individual shards were also performed by LA-ICP-MS in Kiel (with 50 µm diameter craters and <sup>44</sup>Ca as the internal standard), where a total of 39 shards were analysed from the eight tephra units. The large ablation crater used meant that the latter (Kiel) analyses had generally  
20 higher analytical precision (less analytical scatter) and allowed determination of a larger number of elements (up to 40). However, the limited number of glass shards 50 µm or larger in size did not allow analysis of more than 8–10 shards per sample. The analyses from Kiel with Si and Ti concentrations deviating by more than 20 % relative from EPMA data were excluded as they were affected by contamination by mineral  
25 phases during analysis. For both laboratories, analysis of the MPI-DING ATHO-G reference rhyolitic glass (GeoReM, Jochum et al., 2006), under the same conditions, shows that accuracy is good.

The differences between the two LA-ICP-MS methods resulted in different results on trace element concentrations in the tephtras. The systematic difference varies from 1.18

5983

(Kiel/Aberystwyth) for Cs to 0.51 for Ta. The concentrations for most elements obtained in Aberystwyth are higher compared to those from Kiel. The ratios of trace elements, including those which are sensitive to contamination by minerals during analysis (e.g. Zr/Y for pyroxene and amphibole, Sr/Ce for plagioclase) are less variable and generally  
5 agree within 20 % relative between the two labs (e.g. Zr/Y, Ba/Sr, Sr/Ce, Ba/Nb, La/Sm, La/Yb). The reasons for the discrepancy in absolute concentrations is not clear at present. However, because both labs have produced significant amounts of data in the past years contributing to widely used databases in their respective research areas, and the need to compare between the datasets for the different regions, both  
10 sets of data are used here. It is important to note that direct comparison of the absolute trace element concentrations obtained from glass shards in Aberystwyth and Kiel is not straightforward at present. Where comparison of absolute concentrations is required, the trace element data obtained in Aberystwyth are used to compare with the Alaskan tephra, which have been analysed in the same laboratory at similar conditions with  
15 small laser spots (20 µm or less) (e.g. Preece et al., 2011a, b). The data obtained in Kiel are used to compare to Kamchatkan tephra as much of the data for Kamchatka has been determined in this laboratory under the same conditions (e.g. Ponomareva et al., 2013b).

Pb isotope analyses were also performed by LA-ICP-MS at Aberystwyth University on a total of 190 individual glass shards from all tephra deposits (Table S4, Appendix A3.3). Methods used were those described by Westgate et al. (2011). Analyses were performed using 20 µm or 30 µm ablation craters, and calibrated against the Pb isotope ratio from the NIST 612 glass, with analytical accuracy monitored by analysis of USGS glass reference materials. At such relatively small crater diameters, precision  
25 and accuracy is compromised compared to analysis of larger samples (e.g. by solution ICP-MS or large spot sizes using LA-ICP-MS), but this provides reconnaissance data suitable for preliminary interpretations (Westgate et al., 2011a). Full details of all analytical methods and results are given in the Appendix A and the Supplement.

5984

### 3 The El'gygytgyn tephra record

Eight tephra layers were recognized in the main cores (T0–T7), with two present in the pilot cores (T0–T1) (Table 1). The layers are several mm up to 7.4 cm thick. In most layers, the top few mm of the layers appeared reworked, with some mixed in material. The ash horizons are composed of 99 % volcanic material as seen in smear slides.

All layers form distinct tephra horizons separated from each other by several cm to dm of sediment (Fig. 2). Thicknesses were measured in the opened core. Individual tephra in the cores are assigned working names and numbered from top to bottom (E-Tephra T0–T7). Tephra layers have a light grayish to dark brown appearance. They are made up of glass shards that are mainly colorless or pale yellow to brown (Fig. 3). Particle morphologies include highly vesicular pumice, tubular and blocky pumice, bubble-wall shards and non-vesicular platy shards. Igneous crystals are rare in the tephra layers. Shards are up to 400 µm in diameter, but the median diameter is 40 µm. All of the tephra layers have distinct individual characteristics. Glass shards were analyzed from all horizons. More than 900 EMP-analyses on individual glass shards from the eight tephra layers (T0–T7) have been obtained from both laboratories. The eight tephra layers have glass shards that are chiefly rhyolitic to dacitic ( $\text{SiO}_2 > 65$  wt.%), one tephra (T5) has glass shards ranging from rhyolite to basaltic andesite ( $\text{SiO}_2 > 75.7$ –53.7 wt.%) in composition (Fig. 4). The tephra layers are medium to high-K subalkaline (Figs. 4 and 5). All of them show high Cl contents  $> 0.1$  wt.% (Fig. 5). The chemical composition of shard populations in the tephra layers is generally homogeneous, only the compositions of T3 and T5 vary systematically. The tephra layers resemble each other compositionally, but can be distinguished by their major-element composition, such as  $\text{SiO}_2$  and  $\text{K}_2\text{O}$  concentrations (Fig. 5), trace-element composition (Fig. 6), glass shard morphologies, relative stratigraphic position and age.

Twenty six trace-elements were determined from each of the 8 sampled El'gygytgyn tephra layers by LA-ICP-MS, giving analyses from 227 single grains after analyses were filtered to remove those which ablated phenocrysts in the glass (see Pearce

5985

et al., 2002, 2004, 2007). This gave between 10–52 analyses for each tephra. There are many similarities between each of the tephra in their general trace element contents. Except for T5, all samples show a distinct anomaly at Sr and Eu (Fig. 6, Table 3a) indicating fractionation of plagioclase. Using a series of bivariate plots of compatible (in silicic magmas) and incompatible elements it is possible to readily separate most of the tephra (see Fig. 6). Particularly useful are Rb, Ba, Zr, Y, HREE and trace element ratios La/Sm, La/Yb, Ba/La, Ba/Th, which show the single tephra layers to occupy distinct compositional spaces. Tephra T1, T5, and T7 have distinctive trace-element compositions, while Tephra T0, and T2–T4 have very similar trace-element compositions that are distinguished by subtle differences in Ba/La, Ba/Th and La/Nb ratios (Fig. 6). Each of the tephra horizons represents a distinct eruption event or tephra marker, and are described from youngest to the oldest.

#### 3.1 Tephra 0

The youngest tephra visible in the cores was found in the pilot core, as well as cores LZ 1029-8 III and LZ1039-2 III at 1.59–1.61 m and 2.11–2.13 m below lake floor, respectively (Juschus et al., 2007). It is found as a 2 cm thick whitish layer in the cores. The tephra consists of platy, highly vesicular colorless glass shards, up to 160 µm length. Shards in the pilot core (LZ 1029-8) appeared more fine-grained, with a maximum size of 80 µm. The glass population has a homogeneous composition with  $72.8 \pm 0.6$  wt.%  $\text{SiO}_2$  and  $1.8 \pm 0.1$  wt.%  $\text{K}_2\text{O}$  (Fig. 5, Table 2).

#### 3.2 Tephra 1

T1 comprises tephra beds in the pilot core (Juschus et al., 2007), cores LZ1024-9 I, and in cores 5011-1B-1H2 and 5011-1A-1H-3. In the cores the tephra is present as a ca. 1 cm thick layer (Fig. 2). It consists mainly of colourless pumiceous finer-grained shards with a median size of about 40 µm, and some larger ( $< 100$  µm), colorless, highly vesicular shards (Fig. 3). The composition of T1 is homogenous with high  $\text{SiO}_2$  contents

5986



of  $77.7 \pm 0.2$  wt% and medium  $K_2O$  contents of  $2.8 \pm 0.1$  wt%. Within the El'gygytgyn tephra suite, this tephra has the highest  $SiO_2$  content (Figs. 4 and 5; Table 2).

### 3.3 Tephra 2

T2 occurs in cores 5011-1A-8H-1 and 5011-1B-7H-3 as a 0.5 cm silty enrichment in the core (Fig. 2). Glass shards are  $\leq 100 \mu m$ , colorless, and platy with round vesicles (Fig. 3). The horizon is characterized by a bimodal glass shard suite, comprising rhyolitic to rhyodacitic compositions. The  $SiO_2$  content ranges from 77.2 and 72.1 wt%  $SiO_2$ , with  $K_2O$  from 3.1 to 2.4 wt%, FeO from 1.6 to 3.2 wt%, and CaO from 0.9 to 2.2 wt% (Figs. 4 and 5; Table 2).

### 3.4 Tephra 3

T3 was collected from cores 5011-1B-10H und 5011-1A-11H-1, and is 6 cm thick (Fig. 2). It consists of fine-grained, colourless, vesicular shards, with rare brown glass. The layer is finer grained at the bottom and top, and coarser in the middle, and shards are up to  $150 \mu m$  in size. The colorless shards have variable  $SiO_2$  contents from 74.0 to 64.5 wt% (Fig. 4). This, and the variation in MgO concentration from 0.4 to 1.8 wt% and of FeO from 2.5 to 6.1 wt%, suggest eruption from a chemically-zoned magma chamber (Figs. 4 and 5; Table 2).

### 3.5 Tephra 4

This prominent, white, 5 cm thick tephra layer (Fig. 2) occurs in a section of the core that is interpreted as part of a sequence of multiple turbidites, interspersed with deposits associated with larger mass movements (Melles et al., 2012; Sauerbrey et al., 2012). T4 is reworked within these deposits and appears up to three times in the core. This tephra layer consists of colorless tubular pumice, pumiceous and vesicular glass shards (Fig. 3). The median grain size is about  $60 \mu m$ , the largest shards are up to  $250 \mu m$ . T4 is chemically homogeneous, with a rhyolitic composition comprising high

5987

$SiO_2$  ( $71.0 \pm 0.5$  wt%), high  $Na_2O$  ( $5.1 \pm 0.5$  wt%) and low  $K_2O$  ( $2.3 \pm 0.1$  wt%) contents (Fig. 4, Table 2).

### 3.6 Tephra 5

This distinctive 4 cm thick brownish tephra (Fig. 2) is fine-grained with a median shard size of  $40 \mu m$ . It is comprised of brown to greenish platy tricusate glass shards, and highly vesicular colorless shards (Fig. 3). It is fine-grained with fewer than 2% of the shards up to  $80 \mu m$  in size. It has the broadest compositional range of all the tephra beds, with  $SiO_2$  wt% spanning from 75.8 to 53.8 wt% (Figs. 4 and 5). The variation in MgO (0.2–4.0 wt%) and FeO (1.6–11.1 wt%) content suggests this tephra was erupted from a chemically-zoned magma chamber. T5 has the flattest REE profile with the least pronounced Eu anomaly (Fig. 6).

### 3.7 Tephra 6

T6 is  $< 7$  mm thick (Fig. 2), but contains shards up to  $300 \mu m$ . It is comprised of colourless glass shards that range in morphology from stretched and blocky pumice to platy shards (Fig. 3). The blocky pumice has numerous small, round, evenly-sized vesicles, occurring on glass surfaces. Few blocky brown shards were seen, but all displayed the same morphology as the colorless shards. T6 has a homogeneous major-element composition with  $SiO_2$  at  $70.6 \pm 0.5$  wt%,  $K_2O$  at  $2.5 \pm 0.1$  wt%, and relatively high  $Na_2O$  content of  $4.7 \pm 0.3$  wt%. It also has the highest Nb and Ta concentrations of the tephtras, and shows the highest HREE and a relatively flat REE profile, similar to T2, T3 and T4 (Fig. 5).

### 3.8 Tephra 7

Shards in this 4 mm thick white to grey tephra horizon (Fig. 2) are up to  $500 \mu m$  in diameter. They are colorless and comprised of stretched and blocky pumice. Blocky shards contain many evenly distributed vesicles that are generally  $\sim 1 \mu m$  in diameter.

5988

The glass margins show extensive scalloping along the edges. The composition of T7 is homogeneous, with high SiO<sub>2</sub> content ( $77.5 \pm 0.3$  wt%), and with the highest K<sub>2</sub>O content ( $4.0 \pm 0.1$  wt%) of the El'gygytyn tephra. T7 is also distinct in its trace element composition, with the highest Ba, Rb, Th, and LREE, and the lowest Sr and HREE, giving it the steepest REE patterns (Fig. 6).

#### 4 Age of tephra layers

The three parallel sediment cores from Lake El'gygytyn were spliced into a composite core and a high-resolution age model was developed using a multi-proxy approach (Nowaczyk et al., 2013). Magnetostratigraphy provides the tie points for the basic age model (Haltia and Nowaczyk, 2013). To further refine the age model, nine additional stratigraphic parameters were synchronously tuned (Nowaczyk et al., 2013). Ages of the tephra beds in this study were determined from the resulting age-depth model (Nowaczyk et al., 2013) (Table 1).

Independent ages for the tephra layers are not yet available. Due to the age and composition of the tephra layers (low to medium K and datable phenocrysts being absent) a direct date on the tephra layers is difficult, if not impossible. Vesicular glass shards of 63  $\mu$ m and smaller have been dated using a Laser-Ar/Ar-technique, however analyses carried out on tephra layers from deep sea cores using this approach have been problematic (e.g. Hall and Farrell, 1995). An attempt to date the glass shards of some of the tephra layers from Lake El'gygytyn using the glass fission-track method is currently being carried out and may in the future provide independent age constraints (J. A. Westgate, personal communication, 2013).

5989

### 5 Potential sources of the tephra layers


#### 5.1 Continental volcanoes vs. island arcs

From the major-element distribution, the tephra layers from El'gygytyn are characterized by a subalkaline composition (Fig. 4), and likely originate from a subduction-related tectonic setting rather than from intra-continental vents. Even though intra-continental volcanoes in Chukotka are present  $\sim 300$  km from Lake El'gygytyn (Fig. 1), these volcanoes are associated with lava and cinder cones, and their activity was limited to the Cretaceous (Akinin and Miller, 2012), and are thus unlikely sources for the El'gygytyn tephra. Geochemistry of the Lake El'gygytyn tephra layers also suggests the eruptions did not originate from continental volcanoes. Magmas formed in intraplate settings are expected to have high alkalis, LREE, Nb and Ta contents. The trace element data for the Lake El'gygytyn tephra show strong relative enrichment in LIL (Rb, Ba, Cs) in comparison to similar incompatible LREE (La, Ce) and HFS (Nb, Ta) elements. Therefore, the major- and trace-element composition of these tephra beds suggest an island arc origin (Figs. 4–6). The most likely source for these tephra beds are the many volcanoes that collectively comprise the Kurile–Kamchatka–Aleutian–Arcs and Alaska Peninsula, more than a 1000 km away from Lake El'gygytyn (Fig. 1). Similarly, the Pb isotope data for these tephra beds falls within the compositional envelopes defined by known Pb isotopic values from Kamchatkan and Alaskan volcanoes (Fig. 7). Collectively the geochemical data suggest that the Kurile–Kamchatka–Aleutian arcs and Alaska Peninsula volcanoes are the most likely source for the eruptions, and these areas have been active for more than 2 million yr (e.g. Siebert and Simkin, 2002; Preece et al., 1999).

#### 5.2 Island arc: Alaska vs. Kamchatka volcanoes

The predominantly explosive volcanism of the NW Pacific area is related to the subduction of the Pacific Plate under the Eurasian and North America Plates, forming

5990

the Kamchatka–Kurile–Aleutian arcs, and the Alaska Peninsula. The major and trace-element geochemistry of Lake El'gygytgyn tephra falls within the compositional range of both Alaskan and Kamchatkan tephra beds (Figs. 5 and 6). 

### 5.2.1 Alaskan volcanoes

- 5 Alaska is home to over 130 volcanoes, most of which are located in the Aleutian Arc–Alaska Peninsula (AAAP) and the Wrangell volcanic field (e.g. Nye et al., 1998; Fig. 1). Although the Wrangell volcanic field has been active over the last ~25 Ma (Richter et al., 1990), and the AAAP for ~40 Ma (Jicha et al., 2006), most eruptions from these volcanoes are known only by their widespread tephra **due to the almost continuous**
- 10 **erosion of the proximal deposits over the last ~3 Ma years by glaciation.**

Much of this distal tephra record is recorded in the terrestrial landscape within widespread loess deposits of eastern Beringia (e.g. Westgate et al., 1990). To date, well over 100 widely distributed distal tephra beds have been identified and characterized from the interior of Alaska and Yukon (e.g. Preece et al., 1999, 2000, 2011a; Jensen et al., 2008, 2013). Although distances from AAAP volcanoes to Lake El'gygytgyn are great, generally between 1600–2000 km, tephra with comparable distributions have been documented from these volcanoes in the past (e.g. Jensen et al., 2011; Preece et al., 2011b). This suggests that the AAAP could be a potential source for tephra at the study site. With the Wrangell volcanic field downwind and over 2000 km from Lake El'gygytgyn, it seems unlikely that visible tephra from these volcanoes would be present in the lake. However, they were not excluded from geochemical comparisons.

Comparison of major and minor-element geochemistry of Alaskan to El'gygytgyn tephra was two-fold. Firstly, all El'gygytgyn tephra were run through the University of Alberta Tephrochronology Lab searchable database to query for potential correlatives. The database uses a similarity coefficient (SC; Borchardt et al., 1972) as the basis for its search. **To obtain a SC between the unknown and each tephra in the database, the database first calculates a SC between each individual oxide. These SCs are weighed**

5991

**according to each oxide's precision and accuracy (e.g. MnO wt% is often at the detection limit of the EMP and is excluded), and are then used to calculate a single SC between the unknown and each tephra in the database.** To try and compensate for the large geochemical trends some tephra have wherein averages can be misleading, the standard deviation of SiO<sub>2</sub> wt% is also used in this search. Tephra that are comprised of multiple populations also have averages of each population run through the database independently. Generally, a SC of > 0.95 demonstrates some similarity between two samples though does not necessarily indicate a correlative bed. Tephra beds with SC's > 0.90 were further examined visually through Harker diagrams. When the El'gygytgyn tephra **(T0–T7)** were run through the database, no values over 0.93 were obtained except for T1, which had SCs of 0.94 to 0.96 with the Alyeska Pipeline, Gold Run, P13 and other similar, high SiO<sub>2</sub> wt% rhyolites (e.g. Westgate et al., 2009; Jensen et al., 2013; Table B2).

The detailed comparison of major-element geochemistry between the Alaskan and Lake El'gygytgyn tephra suggests there are no **direct** correlations. However, to test the database results and explore the overall characteristics of the unknowns in comparison to tephra sourced in Alaska, a series of prominent widely distributed tephra beds, including Aniakchak, Dawson, VT, Old Crow, Gold Run, GI, PAL, HP and PA, were plotted with the El'gygytgyn tephra (e.g. Kaufman et al., 2012; Preece et al., 1999, 2011a, b; Demuro et al., 2008; Westgate et al., 2009; Jensen et al., 2013; Fig. 5). These tephra beds were chosen based on their **similarity** to the unknowns (e.g. Table B2), and to capture variability in terms of age (ca. 2 Ma to 3.6 ka), and major-element geochemistry (basaltic-andesite to rhyolite). Results indicate that the major-element geochemistry of Lake El'gygytgyn tephra tend to fall within the compositional range exhibited by this selection of Alaskan tephra (Fig. 5). Some slight systematic differences appear to be present: at less than ~75 SiO<sub>2</sub> wt%, MgO, FeO and CaO tend to be higher at any given SiO<sub>2</sub> wt% than the Alaskan beds, while K<sub>2</sub>O and Al<sub>2</sub>O<sub>3</sub> wt% tend to be a little lower. In conclusion, although the major-element geochemistry suggests that, for at least the tephra under ~75 SiO<sub>2</sub> wt%, Alaskan volcanoes may not be the most likely source, **the**

5992



data is inconclusive. Trace-element geochemistry comparisons between Alaska tephra and T0–T7 are also inconclusive, showing complete overlap (Fig. 6).

The lead isotope data ( $^{206}\text{Pb}$ ,  $^{207}\text{Pb}$  and  $^{208}\text{Pb}$ ) offers the most in terms of delineating a possible Alaskan source. The data are broadly similar for all of the tephra beds, except T6, which differs from the other El'gygytgyn tephtras by having the highest  $^{206}\text{Pb}/^{208}\text{Pb}$  and the lowest  $^{207}\text{Pb}/^{208}\text{Pb}$  ratios. When compared with recent Pb isotope data compiled from Kamchatka and Alaska volcanics, the majority of samples sit close to/within the envelope of  $^{206}\text{Pb}/^{208}\text{Pb}$  vs  $^{207}\text{Pb}/^{208}\text{Pb}$  for published data for recent Kamchatka volcanic rocks. T6, however, plots firmly within the Pb isotope field of recent Alaskan volcanic rocks, suggesting a source from further afield is possible (Fig. 7). A plot of known and dated Alaska tephra beds in comparison to T0–T7 illustrates that frequent eruptions from these volcanoes were occurring during deposition of most of the Lake El'gygytgyn tephra (Fig. 8).

## 5.2.2 Kamchatka volcanoes

The Kurile–Kamchatka Volcanic Arc has a total length of 2000 km, is about 400 km wide on the Kamchatka peninsula, and is one of the most active arc segments on earth (Siebert and Simkin, 2002). It has had numerous explosive eruptions, and the largest number of collapse calderas per unit of arc length (Hughes and Mahood, 2008). In the Holocene, more than thirty-seven large volcanic centers and hundreds of monogenetic vents have been active in Kamchatka and about forty-eight volcanoes are known from the Kurile Islands (Gorshkov, 1970; Siebert and Simkin, 2002; Ponomareva et al., 2007). On the Kurile Islands, the eruption history has been reviewed (Ostapenko et al., 1967; Gorshkov, 1970), albeit the research mainly focused on recent explosive eruptions (e.g. Nakagawa et al., 2002; Belousov et al., 2003; Hasegawa et al., 2012). On Kamchatka, where many explosive eruptions resulted in widespread dispersal of tephra-fall deposits, the Holocene eruptions and their sequences are well investigated. Many decades of on land mapping, correlation of tephra layers, determination of ages and magnitudes of eruptions, has lead to a detailed tephrostratigraphic framework with

5993

more than 40 known large explosive eruptions so far (Braitseva et al., 1987, 1995, 1997, 1998; Kir'yanov et al., 1990; Bazanova et al., 2001; Gusev et al., 2003; Ponomareva et al., 2004, 2007; Kyle et al., 2011). Some Holocene Kamchatka tephtras have also been identified off Kamchatka in terrestrial and marine environments on the Bering and Karaginsky Islands (Kyle et al., 2011), in the Okhotsk Sea cores (e.g. Nürnberg and Tiedemann, 2004; Ponomareva et al., 2004; Derkachev et al., 2012) and as far as mainland Asia (Gorbarenko et al., 2002a, b; Ponomareva et al., 2004).

The volcanic history of the early Holocene and the Pleistocene, however, is less well investigated in Kamchatka and the Kurile Islands. Older Pleistocene tephtra have mostly been removed by glaciation and occur only in isolated outcrops. The geological exposure is poor, the erosion rates are high, and the vegetation cover is heavy. Only a few widespread ash layers are known from this time span. Among these beds, one of the largest explosive eruptions is from Plosky volcano, Kamchatka, at 10.2 ka cal. BP (e.g. Braitseva et al., 1995; Ponomareva et al., 2013). There is also the K2 Tephtra at 24.5  $^{14}\text{C}$  ka from the northern part of the Kurile Island, most likely from Nemo Caldera (Braitseva et al., 1995; Melekestev et al., 1997; Derkachev et al., 2012), and Raucha Tephtra at 177 ka from a yet unknown eruption probably in the Karymsky volcanic center (Ponomareva et al., 2013b). As the Pliocene–Pleistocene calderas are far larger than the Holocene calderas, and with much greater thicknesses of proximal pyroclastic deposits (Bindemann et al., 2010), it indicates the associated tephtra layers could be distributed further than those from Holocene eruptions. Yet their record is poorly documented.

The high concentration of tephtra layers in marine sediment cores in the adjacent seas supports the notion of a high eruption frequency on Kamchatka in the Pliocene–Pleistocene. From over 40 records from the Okhotsk Sea, spanning the last 350 ka, a sequence about 22 tephtra layers have been documented, among which are at least nine widespread ash layers (e.g. Gorbarenko et al., 1998, 2000, 2002a, b; Derkachev et al., 2004; Nürnberg and Tiedemann, 2004; Derkachev et al., 2012). Northwestern Pacific deepsea sediments document numerous explosive eruptions over the last five

5994

million years with an increase in the number and thickness of volcanic ash layers from 2.6 Ma (Cao et al., 1995: ODP Leg 145, sites 881, 882, 883 and 884; Prueher and Rea, 2001; ODP 887, 883, 882). Cores taken on the SO201 Leg 2 cruise recovered sediment records spanning the last 180 ka with 14 tephra layers in the Bering Sea and 38 layers in the NW Pacific in Kronotsky Bay and Meiji Seamount. (Dullo et al., 2009; Derkachev et al., 2011). High quality geochemical data on glasses are, however, unavailable for most of the Pleistocene ignimbrites and tephra layers.

Comparison of Pb isotopes, and major-, minor- and trace-element compositions of the known Plio–Pleistocene volcanic eruptions to tephtras T0–T7 show their obvious affinity to Kamchatkan tephra (potentially excluding T6). However, with the exception of T1, there are no obvious correlations to known beds from Kamchatka. To further explore these connections, we look at the activity of the Kamchatka–Kurile arc based on the ages of major caldera forming eruptions (from Bindemann et al., 2010) relative to the Lake El'gygytgyn beds (Fig. 8). These data suggest that indeed caldera forming eruptions were taking place at the time of deposition of the Lake El'gygytgyn tephra beds.

The lower  $K_2O$  wt% of glass shards from tephra layer T0, with an inferred age ca. 45 ka, shows similarities to the composition of tephtras and ignimbrites from South Kamchatka, such as ca. 440 kyr Golygin Ignimbrites belonging to Pauzhetka Caldera (Bindeman et al., 2010) and to Kuril Lake ignimbrites (Ponomareva et al., 2004). Although T0 glasses have a slightly more mafic composition, their similarity to tephra deposits related to the Kurile Lake caldera, formed at 7.6 ka BP, is intriguing. The tephra from this eruption was dispersed over an area of  $\leq 3$  million  $km^2$ , and was found at a distance of 1700 km from the source (Anderson et al., 1998). During this eruption about  $\sim 170 km^3$  of tephra were produced and the eruption ranks among the largest Holocene explosive eruptions on Earth (Ponomareva et al., 2004). The chemical similarity of the T0 glasses makes an older eruption from this volcano the plausible source for T0 tephra. Evidence of such an eruption, however, are yet unreported from on-land or marine sites.

5995

Tephra layer T1 in core 5011 has been correlated to the second layer in the pilot core Lz1024-EL2. The sample from the pilot core is chemically indistinguishable from Raucha Tephra from a terrestrial site in East Russian Arctic, 330 km NW of Lake El'gygytgyn (Ponomareva et al., 2013), and correlates to tephra layers identified in marine Bering Sea and Pacific sediment cores SO 201-2-81/85 (Dullo et al., 2009). The distribution of the tephra thicknesses has been used to suggest that it likely originates from an eruption in the Karymsky Volcanic Center in the Kamchatka volcanic arc, albeit the tephra has not been identified on land (Ponomareva et al., 2013b).

Tephtras T2, T3, T4 and T6 have dacitic to rhyolitic, (with moderate  $K_2O$ ) compositions, and similar trace element patterns, which are only vary slightly in their ratios of highly incompatible elements (e.g. Ba/La, La/Nb). Overall, the compositions are typical for Kamchatka and particularly for centers in the volcanic front around the Karymsky Caldera (Kyle et al., 2010; Ponomareva et al., 2013a). This area has a high density of nested calderas that might be plausible sources for the tephtras. Few of the ignimbrite flows related to these calderas have been dated so far, and no exact match in age and composition between published data and these tephra exists at present. One possible candidate could be the dacitic eruption related to Stena–Sobolny Caldera at 1.13 Ma (Bindeman et al., 2010), which could be correlated to the dacitic T3 tephra with the inferred age ca. 0.9 Ma, although the age difference of 200 ka makes this correlation questionable. T6 has an identical inferred age of 1.78 Ma with ignimbrites related to Karymshina Caldera (Bindeman et al., 2010). However, the composition of the ignimbrites produced by this super eruption show a much more evolved geochemical composition than the glass of T6 (Bindeman et al., 2010).

Dacite-andesitic glasses of tephra T5 imply an andesitic composition for the bulk tephra. Only a few large andesitic eruptions are known in Kamchatka, and all are dated to the Pliocene (3.5–5.7 Ma, Bindeman et al., 2010). These eruptions occurred in the Eastern Volcanic Zone of Kamchatka and in Sredinny Range. None of these eruptions can be directly correlated to T5 tephra, which is dated to 1.4 Ma.

5996

The oldest tephra, T7, has a unique composition and a somewhat uncertain age due to possible sediment disturbance in the cores. This makes its correlation to a possible source problematic. Nevertheless, judging from its geochemistry alone, and assuming the source in Kamchatka, it should be located in a small region of the volcanic arc where compositions of tephra are more alkalic, enriched in LILE and depleted in HREE, as exemplified by Opala Volcano in South Kamchatka (Kyle et al., 2010).

## 6 Conclusions

The eight tephra layers preserved in Lake El'gygytyn sediments provide a unique opportunity to correlate terrestrial and marine climate archives in the Bering Sea and North Pacific region. They also indicate that there is great potential to find distal ash in western Beringian sediments, helping place those archives within a dated framework.

The geochemical data indicate that the source of these tephra beds lie in the subduction zone volcanoes that form the Kurile–Kamchatka–Aleutian Arc and Alaska Peninsula. While major-, minor- and trace-element geochemistry is generally inconclusive in determining the potential source, the lead isotopic data shows that the Kurile–Kamchatka arc is the most likely source for seven of the eight tephra. For T6, an Alaskan source is possible, but there is presently no known tephra that correlates to this layer.

The geochemical composition of the seven other tephra suggests a Kamchatka source, and indeed one, T1, has been correlated to the Raucha tephra, which likely has a Kamchatkan source (Ponomareva et al., 2013b). Even though there is much evidence for numerous highly explosive eruptions, as seen in nested calderas in the Eastern Volcanic zone in Kamchatka, the sequence and age of those explosive events are presently not well constrained. Only a small number of Pleistocene ignimbrites in Kamchatka have been studied with modern analytical tools, and the distal record is limited. Therefore, due to a restricted database available for geochemically fingerprinted Kamchatkan material, none of the remaining Lake El'gygytyn tephra were success-

5997

fully correlated, although potential source volcanoes and caldera complexes can be identified. Additionally, tephra layers described from SO201, SO202, ODP or ICDP cores from the Bering Sea and north Pacific lack ~~geochemical composition of glass shards needed for examining correlations between tephra~~.

Even though the source volcanoes for tephra T0–T7 are not known at this stage, they still offer a unique potential for future correlation of terrestrial and marine sites. The thickness of the Lake El'gygytyn tephra, over 1500 km from potential sources, suggest they are widely distributed, and thus are likely present in numerous depositional settings. The geochemistry presented here will allow for the future identification of these tephra, linking these terrestrial deposits to marine and other terrestrial records, and eventually to their source volcanoes. Ultimately these tephra beds from Lake El'gygytyn provide the basis for a robust tephrostratigraphic framework for western Beringia that we predict will develop quickly now that the presence of tephra beds in this region is known.

## Appendix A

### Methods

#### A1 Petrographic description

All visible tephra layers in the cores were sampled and described petrographically, prior to chemical analysis for major, trace and Pb isotope composition by electron probe microanalysis (EPMA) and laser ablation inductively coupled plasma-mass spectrometry (LA-ICP-MS).

Volcanic ash layers occur in both the pilot cores (LZ 1024, PG1351 and 5011-1) and in the main cores studied (5011A, 5011B, Fig. 2, and Table 1). Tephra layers were identified in the cores directly after opening. Smear slides were taken from every change in lithological composition and checked for volcanic glass shards. All tephra

layers were sampled and freeze dried. Petrologic characteristics of the tephra layers were described from smear slides and polished sections (grain size, mineralogical content). Subsamples for chemical investigations of glass shards were carefully washed in distilled water to sieve off finest grains and dried at 40 °C, mounted in epoxy, polished and carbon coated for electron probe microanalysis (EPMA) analyses.

## A2 Electron probe microanalyses

Glass shards from the tephra layers were analyzed for their major and minor element composition by electron microprobe to gain information about the provenance and enable a robust correlation to existing databases of possible source volcanoes. Analyses were performed using two different electron microprobes, at the University of Alberta, Edmonton, and at GEOMAR, Kiel. These two laboratories host databases for volcanic ash layers from different regions (North America and Kamchatka respectively), which are relevant to the correlation of the El'gygytgyn tephra layers. The INTAV (INQUA International focus group on tephrochronology) inter-comparison of tephrochronology laboratories confirmed the high quality of the microprobe results from both instruments (Kuehn et al., 2011), with both instruments producing data sets that are identical within statistical deviations. In this way the inter-laboratory calibration issues were excluded.

### A2.1 EPMA – University of Alberta, Canada

At the University of Alberta, the major-element geochemical composition of single glass shards were analyzed with a JEOL 8900 superprobe. Analytical conditions were a 15 kV accelerating voltage, 6 nA beam current, and 10 µm beam diameter, with a 20 s peak and 10 s background counting time on all elements. Na, Si and Al were analyzed first to minimize the effects of Na-loss. Standards used for calibration are Lipari rhyolitic obsidian (UA 5831: Si, Al, Na, K) and minerals (tugtupite: Cl; diopside: Ca; willemite: Mn; pyrope: Fe, Mg; ilmenite: Ti). Matrix effects are corrected for using the ZAF correction factor. Internal glass standards ID 3506 (a Lipari obsidian) and Old Crow tephra

5999

were analyzed at the beginning, after every four samples (i.e. ~ 100 shards), and end of each analytical session to monitor quality of the calibration (e.g. Kuehn et al., 2011). Routine internal standard analyses also allow for the comparison of data collected over the course of days to years by providing a means to correct for any small offsets that may be present due to variations in probe conditions over time. A minimum of 25 shards per sample was analyzed to capture true compositional range, and all totals under 90 % were discarded. The data are normalized to 100 % on a volatile-free basis and are presented as weight percent (wt%) in Table S1 in the Supplement. All El'gygytgyn tephra layers have been compared to the University of Alberta Alaskan tephra database, with similarity coefficients being calculated for the most similar known Alaskan tephtras, and these are presented in Table 2.

### A2.2 EPMA – GEOMAR, Kiel, Germany

At GEOMAR the chemical composition of single glass shards – major elements, S, Cl and F – was analyzed with the JEOL JXA 8200 electron microprobe equipped with five wavelength dispersive spectrometers including 3 high sensitivity ones (2 PETH and TAPH). Analytical conditions were 15 kV accelerating voltage, 6 nA beam current and 10 s on peak counting time on Na, 20 s of peak counting time (Si, Al, Fe, Mg, Al, Ca), 30 s (K, Ti, Cl, S), 40 s (Mn and F), with 10 s on background. Analyses were performed with a ~ 5 µm electron beam. Standards used for calibration were natural glasses (Rhyol: Na, Si, Al, K and VGA99: P, Fe, Mg, Ti and Ca,) and minerals (rhodonite, scapolite USNM R6600-1: Mn, S and Cl). Sodium was analyzed first during all sessions; sodium loss was not observed. Internal standards (KN18, VGA99) were measured at the beginning, during and end of each analytical session. Data were corrected for obvious microlite inclusions. To cover the whole range of geochemical compositions at least 20 analyses of the samples were obtained. Data in Table 1 show representative analyses of data normalized to 100 %. Full details on data sets are available on request. The data reduction was done online using CITZAF correction (Armstrong, 1995) and correction control for systematic deviations (if any) from the reference val-

6000

ues analyzed on standard material. These analyses were analyzed at the beginning and the end of each session, and every 60 analyses. Corrections applied over time were minor (< 5 % relative to all elements) and allowed the best possible accuracy and reproducibility over long time spans. All analytical data are presented in Table S3 in the Supplement as wt% oxides.



### Laser ablation ICP-MS analyses

The trace element and Pb isotope composition of individual shards of glass was obtained by laser ablation inductively coupled plasma-mass spectrometry (LA-ICP-MS) in Aberystwyth. The Aberystwyth laboratory provides established analytical set ups for determining the chemical composition of fine grained pumiceous glass shards with a median size of less than 40  $\mu\text{m}$ , and allows for the analysis of a pure glass phase at a spatial resolution of 10–20  $\mu\text{m}$ . In total, 226 single shards were analyzed for their glass trace element concentrations and 190 for their Pb isotopes. The database for rhyolitic tephra from Alaska/Yukon was largely developed with analyses on this instrument (see for example Preece et al., 2011).

Trace element analyses were also performed in the Laser-Ablation Laboratory at CAU-University in Kiel where a total of 39 shards had their trace element composition determined. Some analyses of tephra from the El-Gygytgyn core performed in Kiel have recently been published (Ponomareva et al., 2013) and the database for tephra from Kamchatka has been largely obtained by LA-ICP-MS analyses in the CAU-University laboratories in Kiel.

In both sets of analyses, each laboratory produced data for the MPI-DING glass reference material ATHO-G (data is compared in Table S5). While there are some differences in the two data sets, the data from both laboratories is acceptable for correlation purposes in tephra studies. Both laboratories thus provide data which can be compared to the existing databases from both Alaskan and Kamchatkan volcanoes. Unfortunately, because of the differences in the methods employed for the ablation

6001

of the shards which were analysed, and in internal standardization, the two data sets determined on somewhat different materials, and cannot be directly compared.

#### A3.1 LA-ICP-MS – Kiel

Trace elements in glasses were analysed by laser ablation – inductively coupled plasma – mass spectrometry (LA-ICP-MS) using a 193 nm Excimer laser with a large volume ablation cell (ETH Zürich, Switzerland) coupled with a quadrupole-based ICP-MS (Agilent 7500s) at the Institute of Geosciences, CAU Kiel, Germany. In situ microsampling was done with 50  $\mu\text{m}$  pit size and 10 Hz pulse frequency at 8.5  $\text{Jcm}^{-2}$  fluence. The generated aerosol was transported with 0.75  $\text{Lmin}^{-1}$  He and mixed with 0.6  $\text{Lmin}^{-1}$  Ar prior to introduction into the ICP. The ICP-MS was operated under standard conditions at 1500 W and optimized for low oxide formation (typically  $\text{ThO}^+/\text{Th}^+ \leq 0.4\%$ ). The GLITTER software package (Access Macquarie Ltd.) was used for data reduction of the time-resolved measurements. The blank signal was measured 20 s prior to each ablation and used for calculation of the actual detection limits. For sample data integration the time window up to 40 s (depending on size of glass shard) was individually adjusted for each run. Calcium (44  $m/z$ ) was used for internal standardization utilizing pre-analyzed data from electron probe microanalysis (EPMA). Mass numbers analyzed for every element are listed in Table S4 as is a summary of instrument operating conditions. The NIST 612 glass (Jochum et al., 2011) and MPI-DING KL-2G (for Ti) were used for calibration of the integrated raw data and re-analysed in triplicate with every batch of 20 sample acquisitions. International rock glass standards (USGS BCR-2G and MPI-DING glass KL-2G and ATHO-G) (Jochum et al., 2006; GEOREM, 2012) have been analysed as unknown samples in one series with glass samples for check of accuracy (see auxiliary data in Ponomareva et al., 2013b). Analytical precision of five to ten runs of the standard glasses was < 5 % for most elements during one session. To exclude analyses contaminated by possible entrapment of crystal phases, additional quality test has been applied by comparing Si and Ti concentrations measured by LA-ICP-MS with those obtained by EMPA on the

6002



same glass shard. Analysis were accepted as representative for pure glass if both Si and Ti concentrations measured by LA-ICP-MS and EPMA agreed within 20 % relative. The final LA-ICP-MS data represent background-subtracted averages which passed the quality test and are given in Table S6.

### 5 A3.2 LA-ICP-MS – Aberystwyth

Laser ablation ICP-MS analyses were performed on a range of samples in the Institute of Geography and Earth Sciences, Aberystwyth University using a Coherent GeoLas ArF 193 nm Excimer laser ablation system coupled to a Thermo Finnegan Element 2 sector field ICP-MS. Trace element data was collected for individual shards using 20  $\mu\text{m}$  and 14  $\mu\text{m}$  diameter ablation craters at a laser energy of 10  $\text{Jcm}^{-2}$  and a repetition rate of 5 Hz over a 24 s acquisition. Crater size was varied because of the size of individual glass shards to be analyzed. The minor  $^{29}\text{Si}$  isotope was used as the internal standard, and the average concentration of  $\text{SiO}_2$  for each sample (determined by EPMA) was used to calibrate each analysis, after normalization to an anhydrous basis. The NIST 612 reference glass was used for calibration, with concentrations given in Pearce et al. (1997), and a fractionation factor was applied to the data to account for analytical bias introduced related to the different matrices of the reference standard and the sample (see Pearce et al., 2011). Further details of the set up procedures and discussion of the precisions and accuracies etc. can be found in Pearce et al. (1996, 1999, 2002, 2004a, 2007, 2011), and ICP-MS and laser operating conditions are summarized in Table S4. The MPI-DING reference glass ATHO-G (Jochum et al., 2006; Jochum and Stoll, 2008) was analyzed as an unknown under the same operating conditions at the same time, and these analyses are given in Table S5. Analytical precision is typically between  $\pm 5$ –10 % (depending on concentration and crater diameter), and accuracy is typically around  $\pm 5$  %, when compared with the published GeoReM concentrations for ATHO-G. All individual shard trace element data are presented in Table S7.

6003

### A3.3 Lead isotopes

Pb isotope compositions were determined by LA-ICP-MS from individual glass shards for all 7 samples at Aberystwyth University. For the Pb isotope analysis the Thermo Finnegan Element 2 sector field ICP-MS was operated in low resolution mode, and He was used as the sample gas ( $0.825 \text{ Lmin}^{-1}$ ) made up with Ar ( $\sim 0.7 \text{ Lmin}^{-1}$ ). The instrument was optimized to give the greatest sensitivity for  $^{208}\text{Pb}$  from the NIST 612 reference glass. Instrument operating conditions are given in Table S4. Where possible, analyses were performed using a 30  $\mu\text{m}$  diameter laser beam which ablated to a depth of about 20  $\mu\text{m}$ , although for some samples a 20  $\mu\text{m}$  diameter beam had to be used to avoid ablation of mounting resin.

Calibration was achieved from 10 repeat analyses of NIST 612 at the start and end of each set of analyses using the Pb isotopic ratios from GeoReM (see Jochum et al., 2005; Jochum and Stoll, 2008). Gas blanks (5 repeats) were measured before and after each of the standard analyses, and also between samples. Twenty individual glass shards were analyzed in each unknown, and only 2 unknowns were analyzed between the NIST reference materials in each set of analyses. This process ensured that reference materials (for calibration and to monitor any instrumental drift) were analyzed at intervals of typically around 1.5 h. Spectra obtained from the NIST 612 glass (30  $\mu\text{m}$  ablation craters) gave about 270 000 cps for  $^{208}\text{Pb}$  (38.57 ppm Pb), and from the unknown glass shards (with an average of  $\sim 12$  ppm Pb) count rates were lower, averaging  $\sim 29$  000 cps, a result of poorer ablation characteristics of natural glasses and the need to use a 20  $\mu\text{m}$  diameter crater for many analyses. For each analysis the masses 201, 204, 206, 207, and 208 were measured sequentially and averaged over 100 scans.  $^{204}\text{Pb}$  suffers interference from  $^{204}\text{Hg}$ , and thus  $^{201}\text{Hg}$  was measured to allow a correction for this. Mass bias in the ICP-MS was calculated from the  $^{206}\text{Pb}/^{208}\text{Pb}$  isotope ratio of the NIST glass after blank subtraction ( $< 100$  cps on  $^{208}\text{Pb}$ ), and using this, and the relative isotope abundances of Hg (Rosman and Taylor, 1997), the calculated contribution of  $^{204}\text{Hg}$  (based on the  $^{201}\text{Hg}$  intensity) was subtracted from

6004

the intensity of the mass 204 peak to leave only  $^{204}\text{Pb}$ . Mercury is present as a trace contaminant in the Ar used in ICP-MS, as well as being present in the NIST standard and in natural volcanic glasses, thus any attempt to measure  $^{204}\text{Pb}$  in glasses must compensate for this Hg interference to the  $^{204}\text{Pb}$  signal. Once the correction for  $^{204}\text{Hg}$  had been applied, calibration was achieved using the Pb isotope ratios given by Jochum et al. (2005), and included correction for any instrument drift during each run. Further considerations of this technique are given in Westgate et al. (2011). Table S8 shows the determined Pb isotope ratios for 2 USGS glass reference materials TB-1G and BCR-2G, with the Pb isotope composition taken from GeoReM (see Jochum and Stoll, 2008). The Pb isotope ratios determined by LA-ICP-MS analyses are typically within  $\pm 0.3\%$  of the reference isotope ratios and analytical precision for ratios between  $^{206}\text{Pb}$ ,  $^{207}\text{Pb}$  and  $^{208}\text{Pb}$  are generally better than  $\pm 1\%$ . Ratios to  $^{204}\text{Pb}$  however show worse precision, at about  $\pm 1.5\%$  for TB-1G, about  $\pm 4.5\%$  for BCR-2G, despite good accuracy, and this reflects the noise on the Hg signal, which makes a significant contribution to the  $^{204}\text{Pb}$  signal, particularly at low concentrations and count rates. In the case of BCR-2G, the  $^{204}\text{Hg}$  correction accounts for almost 70% of the signal at mass 204, leaving only a few hundred  $^{204}\text{Pb}$  counts. Considering these issues, the size of the ablation craters, and the speed with which analyses can be performed, these data are useful and appropriate for reconnaissance studies of Pb isotope ratios in tephra deposits (see Westgate et al., 2011).

The Pb isotope from 20 individual grains of glass from each of the tephra layers were determined by LA-ICP-MS (see Westgate et al., 2011). Because of a generally low signal and interference from Hg on  $^{204}\text{Pb}$ , all other isotope ratios to  $^{204}\text{Pb}$  are very noisy, (RSDs on these ratios of  $\sim \pm 10\%$ ). However, for the  $^{206}\text{Pb}/^{208}\text{Pb}$  and  $^{207}\text{Pb}/^{208}\text{Pb}$  ratios precisions are better than 1%, and these analyses can provide a reconnaissance interpretation of Pb isotope ratios, and may provide information on possible sources. It should be noted that only the average data is considered here.

6005

**Supplementary material related to this article is available online at  
<http://www.clim-past-discuss.net/9/5977/2013/cpd-9-5977-2013-supplement.zip>.**

*Acknowledgements.* Funding for this research was provided by the International Continental Scientific Drilling Program (ICDP), the US National Science Foundation (NSF), the German Federal Ministry of Education and Research (BMBF), Alfred Wegener Institute (AWI) and Geo-ForschungsZentrum Potsdam (GFZ), the Russian Academy of Sciences Far East Branch (RAS FEB), the Russian Foundation for Basic Research (RFBR), and the Austrian Federal Ministry of Science and Research (BMWF). The Russian GLAD 800 drilling system was developed and operated by DOSECC Inc., the down hole logging was performed by the ICDP-OSG, and LacCore, at the University of Minnesota, handled core curation.

C. v. d. B., M. P. and V. P. received support by the KALMAR Project, a joint German–Russian project funded by the German Federal Ministry of Education and Research (BMBF). B. J. and D. F. received funding from Natural Sciences and Engineering Research Council of Canada (NSERC).

The service charges for this open access publication have been covered by a Research Centre of the Helmholtz Association.

## References

- Akinin, V. V. and Miller, E. L.: Evolution of calc-alkaline magmas of the Okhotsk–Chukotka Volcanic Belt, *Petrology*, 19, 237–277, 2012.
- Armstrong, J. T.: CITZAF – a package of corrections for the quantitative electron microbeam X-ray analysis of thick polished materials, thin films and particulates, *Microb. Anal.*, 4, 177–200, 1995.
- Bazanova, L. I. and Pevzner, M. M.: Khangar: one more active volcano in Kamchatka, *Transactions (Doklady) of the Russian Academy of Sciences, Earth Sci.*, 377A, 307–310, 2001.
- Belousov, A. B., Belousova, M. G., Grushin, S. Y., and Krestov, P. B.: Historic eruptions of the Chikurachki volcano (Paramushir, Kurile Islands), *Volcanol. Seismol.*, 3, 15–34, 2003 (in Russian with English abstract).

6006

- Bindeman, I. N., Leonov, V. L., Izbekov, P. E., Ponomareva, V. V., Watts, K. E., Shipley, N. K., Perepelov, A. B., Bazanova, L. I., Jicha, B. R., Singer, B. S., Schmitt, A. K., Portnyagin, M. V., and Chen, C. H.: Large-volume silicic volcanism in Kamchatka: Ar-Ar, U-Pb ages and geochemical characteristics of major pre-Holocene caldera-forming eruptions, *J. Volcanol. Geoth. Res.*, 189, 57–80, 2010.
- 5 Borchardt, G. A., Aruscavage, P. J., and Millard Jr., H. T.: Correlation of the Bishop Ash, a Pleistocene marker bed, using instrumental neutron activation analysis, *J. Sediment. Res.*, 42, 301–306, 1972.
- Braitseva, O. A., Litasova, S. N., and Ponomarenko, A. K.: Application of tephrochronological method for dating of the key archaeological site in Eastern Kamchatka, *Volcanol. Seismol.*, 10 5, 507–514, 1987.
- Braitseva, O. A., Melekestsev, I. V., Ponomareva, V. V., and Sulerzhitsky, L. D.: The ages of calderas, large explosive craters and active volcanoes in the Kuril–Kamchatka region Russia, *B. Volcanol.*, 57, 383–402, 1995.
- 15 Braitseva, O. A., Ponomareva, V. V., Sulerzhitsky, L. D., Melekestsev, I. V., and Bailey, J. C.: Holocene key-marker tephra layers in Kamchatka, Russia, *Quaternary Res.*, 47, 125–139, 1997.
- Braitseva, O. A., Bazanova, L. I., Melekestsev, I. V., and Sulerzhitsky, L. D.: Largest Holocene eruptions of Avachinsky volcano, Kamchatka, *Volcanol. Seismol.*, 20, 1–27, 1998.
- 20 Brigham-Grette, J., Melles, M., Minyuk, P., and Scientific Party: Overview and significance of a 250 ka paleoclimate record from El'gygytgyn Crater Lake, NE Russia, *J. Paleolimnol.*, 37, 1–16, 2007.
- Cao, L. Q., Arculus, R. J., and McKelvey, B. C.: Geochemistry and petrology of volcanic ashes recovered from sites 881 through 884: a temporal record of Kamchatka and Kurile volcanism, in: *Proceedings of the Ocean Drilling Program, Scientific Results*, 145, edited by: Rea, D. K., Scholl, D. W., and Allan, J. F., 345–381, 1995.
- Davies, S. M., Wastegård, S., and Wohlfarth, B.: Extending the limits of the Borrobol Tephra to Scandinavia and detection of new early Holocene tephtras, *Quaternary Res.*, 59, 345–352, 2003.
- 30 Davies, S. M., Abbott, P. M., Pearce, N. J. G., Wastegård S., and Blockley, S. P. E.: Integrating the INTIMATE records using tephrochronology: rising to the challenge, *Quaternary Sci. Rev.*, 36, 11–27, doi:10.1016/j.quascirev.2011.04.005, 2012.

6007

- Demuro, M., Roberts, R. G., Froese, D. G., Arnold, L. J., Brock, F., and Bronk Ramsey, C.: Optically stimulated luminescence dating of single and multiple grains of quartz from perennially frozen loess in western Yukon Territory, Canada: comparison with radiocarbon chronologies for the late Pleistocene Dawson tephra, *Quat. Geochronol.*, 3, 346–364, 2008.
- 5 Derkachev, A. N., Nikolaeva, N. A., and Gorbarenko, S. A.: The peculiarities of supply and distribution of clastogenic material in the Sea of Okhotsk during late Quaternary, *Russ. J. Pac. Geol.*, 23, 37–52, 2004.
- Derkachev, A. N., Portnyagin, M. V., Ponomareva, V. V., Gorbarenko, S., Malakhov, M., Nürnberg, D., Riethdorf, J. R., Tiedemann, R., and van den Bogaard, C.: Marker tephra layers in the Holocene–Pleistocene deposits of the Bering Sea and the north-western Pacific Ocean, in: *KALMAR – Second Bilateral Workshop on Russian–German Cooperation on Kurile–Kamchatka and Aleutian Marginal Sea–Island Arc Systems*, 16 May–20 May 2011, Trier, 2011.
- 10 Derkachev, A. N., Nikolaeva, N. A., Gorbarenko, S.A., Harada, N., Sakamoto, T., Iijima, K., Sakhno, V. G., Hua Hua, L. V., and Wang, K.: Characteristics and ages of tephra layers in the central Okhotsk Sea over the last 350 kyr, *Deep-Sea Res. Pt. II*, 61–64, 179–192, 2012.
- Doerfler, W., Feeser, I., van den Bogaard, C., Dreibrodt, S., Erlenkeuser, H., Kleinmann, A., and Merkt, J.: A high-quality annually laminated sequence from Lake Belau, Northern Germany: revised chronology and its implications for palynological and tephrochronological studies, *Holocene*, 22, 1413–1426, doi:10.1177/0959683612449756, 2012.
- Dugmore, A.: Icelandic volcanic ash in Scotland, *Scot. Geogr. Mag.*, 105, 168–172, 1989.
- Dullo, C., Baranov, B., and van den Bogaard, C.: *RV Sonne Fahrtbericht, Cruise Report SO201-2: KALMAR (Kurile–Kamchatka and Aleutian Marginal Sea–Island Systems): geodynamic and climate interaction in space and time*, IFM-GEOMAR Report, 35, 1–233, 2009.
- 15 Froese, D. G., Westgate, J. A., Sanborn, P. T., Reyes, A. V., and Pearce, N. J. G.: The Klondike goldfields and Pleistocene environments of Beringia, *GSA Today*, 19, 4–10, doi:10.1130/GSATG54A.1, 2009.
- George, R. M. M., Turner, S. P., Hawkesworth, C. J., Bacon, C. R., Nye, C., Stelling, P., and Dreher, S.: Chemical versus temporal controls on the evolution of tholeiitic and calc-alkaline magmas at two volcanoes in the Alaska–Aleutian arc, *J. Petrol.*, 45, 203–219, 2004.
- 30 Giaccio, B., Nomade, S., Wulf, S., Isaia, R., Sottili, G., Cavuoto, G., Galli, P., Messina, P., Sposato, A., Sulpizio, R., and Zanchetta, G.: The late MIS 5 Mediterranean tephra mark-

6008

- ers: a reappraisal from peninsular Italy terrestrial records, *Quaternary Sci. Rev.*, 56, 31–45, doi:10.1016/j.quascirev.2012.09.009, 2012.
- Gorbarenko, S. A., Chekhovskaya, M. P., and Southon, J. R.: Detailed environmental changes of the Sea of Okhotsk central part during the last glaciation-Holocene, *Oceanology*, 38, 277–280, 1998.
- Gorbarenko, S. A., Derkachev, A. N., Astakhov, A. S., Southon, J. R., Nuernberg, D., and Shapovalov-Chuprynin, V. V.: Lithostratigraphy and tephrochronology of the upper Quaternary sediments of the Sea of Okhotsk, Tikhookean. *Geol.*, 19, 58–72, 2000 (in Russian).
- Gorbarenko, S. A., Khusid, T. A., Basov, I. A., Oba, T., Southon, J. R., and Koizumi, I.: Glacial Holocene environment of the southeastern Okhotsk Sea: evidence from geochemical and palaeontological data, *Palaeo*, 3, 237–263, 2002a.
- Gorbarenko, S. A., Nuernberg, D., Derkachev, A. N., Astachov, A. S., Southon, J. R., and Kaiser, A.: Magnetostratigraphy and tephrochronology of the Upper Quaternary sediments in the Okhotsk Sea: implication of terrigenous, volcanogenic and biogenic matter supply, *Mar. Geol.*, 183, 107–129, 2002b.
- Gorshkov, G. S.: Structure of the Kurile Arc, in: *Volcanism and the Upper Mantle*, Springer US, 1–6, 1970.
- Grönvold, K., Oskarsson, N., Johnsen, S. J., Clausen, H. B., Hammer, C. U., Bond, G., and Bard, E.: Ash layers from Iceland in the Greenland GRIP ice core correlated with oceanic and land sediments, *Earth Planet. Sc. Lett.*, 135, 149–155, 1995.
- Gurov, E. P., Valter, A. A., Gurova, E. P., and Serebrennikov, A. I.: Explosion meteorite crater El'gygytgyn in Chukotka, *Dokl. Akad. Nauk SSSR+*, 240, 1407–1410, 1978.
- Gurov, E. P., Koeberl, C., and Yamnichenko, A.: El'gygytgyn impact crater, Russia: structure, tectonics, and morphology, *Meteorit. Planet. Sci.*, 42, 307–319, 2007.
- Gusev, A. A., Ponomareva, V. V., Braitseva, O. A., Melekestsev, I. V., and Sulerzhitsky, L. D.: Great explosive eruptions on Kamchatka during the last 10,000 years: self-similar irregularity of the output of volcanic products, *J. Geophys. Res.*, 108, 2126, doi:10.1029/2001JB000312, 2003.
- Haltia, E. M. and Nowaczyk, N. R.: Magnetostratigraphy of sediments from Lake El'gygytgyn ICDP Site 5011-1: paleomagnetic age constraints for the longest paleoclimate record from the continental Arctic, *Clim. Past Discuss.*, 9, 5077–5122, doi:10.5194/cpd-9-5077-2013, 2013.

6009

- Hall, C. M. and Farrell, J. W.: Laser  $^{40}\text{Ar}/^{39}\text{Ar}$  Ar ages of tephra from Indian Ocean deep-sea sediments: tie points for the astronomical and geomagnetic polarity time scales, *Earth Planet. Sc. Lett.*, 133, 327–338, 1995.
- Hasegawa, T., Nakagawa, M., Yoshimoto, M., Ishizuka, Y., Hirose, W., Seki, S., Ponomareva, V., and Alexander, R.: Tephrostratigraphy and petrological study of Chikurachki and Fuss volcanoes, western Paramushir Island, northern Kurile Islands: evaluation of Holocene eruptive activity and temporal change of magma system, *Quatern. Int.*, 246, 278–297, doi:10.1016/j.quaint.2011.06.047, 2012.
- Hopkins, D. M.: *The Bering Land Bridge*, Stanford University Press, Stanford, CA, 1967.
- Hughes, G. R. and Mahood, G. A.: Tectonic controls on the nature of large silicic calderas in volcanic arcs, *Geology*, 36, 627–630, doi:10.1130/G24796A.1, 2008.
- Hultén, E.: *Outline of the History of Arctic and Boreal Biota During the Quaternary Period*, Lehre J Cramer, New York, 1937.
- Jensen, B., Froese, D., Preece, S., Westgate, J., and Stachel, T.: An extensive middle to late Pleistocene tephrochronologic record from east-central Alaska, *Quaternary Sci. Rev.*, 27, 411–427, 2008.
- Jensen, B. J. L., Preece, S. J., Lamothe, M., Pearce, N. J. G., Froese, D. G., Westgate, J. A., Schaefer, J., and Begét, J.: The variegated (VT) tephra: a new regional marker for middle to late marine isotope stage 5 across Yukon and Alaska, *Quatern. Int.*, 246, 312–323, doi:10.1016/j.quaint.2011.06.028, 2011.
- Jensen, B. J. L., Pyne-O'Donnell, S., Plunkett, G., Froese, D. G., Hughes, P., Pilcher, J. R., and Hall, V. A.: Intercontinental distribution of an Alaskan volcanic ash, Abstract V43B-2832 of the AGU Fall Meeting, San Francisco, 3–7 December 2012.
- Jensen, B. J. L., Reyes, A. V., Froese, D. G., and Stone, D. B.: The Palisades is a key reference site for the middle Pleistocene of eastern Beringia: new evidence from paleomagnetism and regional tephrostratigraphy, *Quaternary Sci. Rev.*, 63, 91–108, doi:10.1016/j.quascirev.2012.11.035, 2013.
- Jicha, B. R., Singer, B. S., Brophy, J. G., Fournelle, J. H., Johnson, C. M., Beard, B. L., Lapen, T. J., and Mahlen, N. J.: Variable impact of the subducted slab on Aleutian island arc magma sources: evidence from Sr, Nd, Pb, and Hf isotopes and trace element abundances, *J. Petrol.*, 45, 1845–1875, 2004.

6010

- Jicha, B. R., Scholl, D. W., Singer, B. S., Yogodzinski, G. M., and Kay, S. M.: Revised age of Aleutian Island Arc formation implies high rate of magma production, *Geology*, 34, 661–664, doi:10.1130/G22433.1, 2006.
- Jochum, K.-P. and Stoll, B.: Reference materials for elemental and isotopic analysis by LA-(MC)-ICP-MS: successes and outstanding needs, in: *Laser Ablation-ICP-MS in the Earth Sciences, Current Practices and Outstanding Issues*, edited by: Sylvester, P., Mineralogical Association of Canada (MAC) Short Course Series, Vancouver, 147–168, 2008.
- Jochum, K.-P., Nohl, U., Herwig, K., Lammel, E., Stoll, B., and Hofmann, A. W.: GeoReM: a new geochemical database for reference materials and isotopic standards, *Geostand. Geoanal. Res.*, 29, 333–338, 2005.
- Jochum, K.-P., Stoll, B., Herwig, K., Willbold, M., Hofmann, A. W., Amini, M., Aarburg, S. E., Abouchami, W., Hellebrand, E., Mocek, B., Raczek, I., Stracke, A., Alard, O., Bouman, C., Becker, S., Ducking, M., Bratz, H., Klemd, R., de Bruin, D., Canil, D., Cornell, D., de Hoog, C. J., Dalpe, C., Danyushevsky, L., Eisenhauer, A., Gao, Y. J., Snow, J. E., Goschopf, N., Gunther, D., Latkoczy, C., Guillong, M., Hauri, E. H., Hofer, H. E., Lahaye, Y., Horz, K., Jacob, D. E., Kassemann, S. A., Kent, A. J. R., Ludwig, T., Zack, T., Mason, P. R. D., Meixner, A., Rosner, M., Misawa, K. J., Nash, B. P., Pfander, J., Premo, W. R., Sun, W. D. D., Tiepolo, M., Vannucci, R., Vennemann, T., Wayne, D., and Woodhead, J. D.: MPI-DING reference glasses for in situ microanalysis: new reference values for element concentrations and isotope ratios, *Geochem. Geophys. Geosy.*, 7, Q02008, doi:10.1029/2005GC001060, 2006.
- Jochum, K. P., Weis, U., Stoll, B., Kuzmin, D., Yang, Q., Raczek, I., Jacob, D. E., Stracke, A., Birbaum, K., Frick, D. A., Günther, D., and Enzweiler, J.: Determination of reference values for NIST SRM 610–617 glasses following ISO guidelines, *Geostand. Geoanal. Res.*, 35, 397–429, doi:10.1111/j.1751-908 X.2011.00120.x, 2011.
- Juschus, O., Melles, M., Gebhardt, A. C., and Niessen, F.: Late Quaternary mass movement events in Lake El'gygytgyn, north-eastern Siberia, *Sedimentology*, 56, 2155–2174, doi:10.1111/j.1365-3091.2009.01074.x, 2009.
- Kaufman, D. S., Jensen, B. J. L., Reyes, A. V., Schiff, C. J., Froese, D. G., and Pearce, N. J. G.: Late Quaternary tephrostratigraphy, Ahklun Mountains, SW Alaska, *J. Quaternary Sci.*, 27, 344–359, doi:10.1002/jqs.1552, 2012.
- Kepezhinskas, P., McDermott, F., Defant, M. J., Hochstaedter, A., Drummond, M. S., Hawkesworth, C. J., Koloskov, A., Maury, R. C., and Bellon, H.: Trace element and Sr-Nd-Pb

6011

- isotopic constraints on a three-component model of Kamchatka Arc petrogenesis, *Geochim. Cosmochim. Ac.*, 61, 577–600, 1997.
- Kir'yanov, V. Y., Egorova, I. A., and Litasova, S. N.: Volcanic ash on Bering Island (Commander Islands) and Kamchatkan Holocene eruptions, *Volcanol. Seismol.*, 8, 850–868, 1990.
- Kuehn, S. C., Froese, D. G., Shane, P. A. R., and INTAV Intercomparison Participants: The INTAV intercomparison of electron-beam microanalysis of glass by tephrochronology laboratories: results and recommendations, *Quatern. Int.*, 246, 19–47, doi:10.1016/j.quaint.2011.08.022, 2011.
- Kyle, P. R., Ponomareva, V. V., and Rourke-Schluep, R.: Geochemical characterization of marker tephra layers from major Holocene eruptions in Kamchatka, Russia, *Int. Geol. Rev.*, 53, 1059–1097, 2011.
- Lane, C. S., Chorn, B. T., and Johnson, T. C.: Ash from the Toba supereruption in Lake Malawi shows no volcanic winter in East Africa at 75 ka, *P. Natl. Acad. Sci USA*, 110, 8025–8029, doi:10.1073/pnas.1301474110, 2013.
- Layer, P.: Argon<sup>40</sup>/argon<sup>39</sup> age of the Elgygytgyn impact event, Chukotka, Russia, *Meteorit. Planet. Sci.*, 35, 591–599, 2000.
- Le Bas, M., Le Maitre, R., Streckeisen, A., and Zanettin, B.: A chemical classification of volcanic rocks based on the total alkali–silica diagram, *J. Petrol.*, 27, 745–750, 1986.
- Melekestsev, I. V., Volynets, O. N., and Antonov, A. Y.: Nemo III Caldera (Onekotan, I., the Northern Kuriles): structure, <sup>14</sup>C age, dynamics of the caldera-forming eruption, evolution of juvenile products, *Volcan. Seism.*, 19, 41–64, 1997.
- Melles, M., Brigham-Grette, J., Minyuk, P., Koeberl, C., Andreev, A., Cook, T., Fedorov, G., Gebhardt, C., Haltia-Hovi, E., Kukkonen, M., Nowaczyk, N., Schwamborn, G., Wennrich, V., and the El'gygytgyn Scientific Party: The El'gygytgyn Scientific Drilling Project – conquering Arctic challenges through continental drilling, *Sci. Drilling*, 11, 29–40, 2011.
- Melles, M., Brigham-Grette, J., Minyuk, P. S., Nowaczyk, N. R., Wennrich, V., DeConto, R. M., Anderson, P. M., Andreev, A. A., Coletti, A., Cook, T. L., Haltia-Hovi, E., Kukkonen, M., Lozhkin, A. V., Rosèn, P., Tarasov, P., Vogel, H., and Wagner, B.: 2.8 million years of Arctic climate change from Lake El'gygytgyn, NE Russia, *Science*, 337, 315–320, doi:10.1126/science.1222135, 2012.
- Minyuk, P. S. and Ivanov, Y. Y.: The Brunhes–Matuyama boundary in Western Beringia: a review, *Quaternary Sci. Rev.*, 30, 2054–2068, doi:10.1016/j.quascirev.2010.06.008, 2011.

6012



- Myers, J. D. and Marsh, B. D.: Aleutian lead isotopic data: additional evidence for the evolution of lithospheric plumbing systems, *Geochem. Cosmochim. Ac.*, 51, 1833–1842, 1987.
- Nakagawa, M., Ishizuka, Y., Kudo, T., Yoshimoto, M., Hirose, W., Ishizaki, Y., Gouchi, N., Katsui, Y., Solovyov, A. W., Steinberg, G. S., and Abdurakhmanov, A. I.: Tyatya volcano, southwestern Kuril arc: recent eruptive activity inferred from widespread tephra, *Isl. Arc*, 11, 236–254, 2002
- Nürnberg, D. and Tiedemann, R.: Environmental change in the Sea of Okhotsk during the last 1.1 million years, *Paleoceanography*, 19, PA4011, doi:10.1029/2004PA001023, 2004.
- Nowaczyk, N. R., Haltia, E. M., Ulbricht, D., Wennrich, V., Sauerbrey, M. A., Rosén, P., Vogel, H., Francke, A., Meyer-Jacob, C., Andreev, A. A., and Lozhkin, A. V.: Chronology of Lake El'gygytgyn sediments, *Clim. Past Discuss.*, 9, 3061–3102, doi:10.5194/cpd-9-3061-2013, 2013.
- Nye, C. J., Queen, K., and McCarthy, A. M.: Volcanoes of Alaska, Alaska Division of Geological and Geophysical Surveys Information Circular IC 0038, 1998.
- Ostapenko, V. F., Fedorchenko, V. I., and Shilov, V. N.: Pumices, ignimbrites and rhyolites from the Great Kurile Arc, *B. Volcanol.*, 30, 81–92, 1967.
- Pearce, N. J. G., Westgate, J. A., and Perkins, W. T.: Developments in the analysis of volcanic glass shards by Laser Ablation ICP-MS: quantitative and single internal standard-multi-element methods, *Quatern. Int.*, 34–36, 213–227, 1996.
- Pearce, N. J. G., Perkins, W. T., Westgate, J. A., Gorton, M. P., Jackson, S. E., Neal, C. R., and Chenery, S. P.: A compilation of new and published major and trace element data for NIST SRM 610 and NIST SRM 612 glass reference materials, *Geostandard. Newslett.*, 21, 115–144, 1997.
- Pearce, N. J. G., Westgate, J. A., Perkins, W. T., Eastwood, W. J., and Shane, P. A. R.: The application of laser ablation ICP-MS to the analysis of volcanic glass shards from tephra deposits: bulk glass and single shard analysis, *Global Planet. Change*, 21, 151–171, 1999.
- Pearce, N. J. G., Eastwood, W. J., Westgate, J. A., and Perkins, W. T.: The composition of juvenile volcanic glass from the c. 3,600 B.P. Minoan eruption of Santorini (Thera), *J. Geol. Soc. London*, 159, 545–556, 2002.
- Pearce, N. J. G., Westgate, J. A., Perkins, W. T., and Preece, S. J.: The application of ICP-MS methods to tephrochronological problems. *Appl. Geochem.*, 19, 289–322, 2004a.
- Pearce, N. J. G., Westgate, J. A., Preece, S. J., Eastwood, W. J., and Perkins, W. T.: Identification of Aniakchak (Alaska) tephra in Greenland ice core challenges the 1645

6013

- BC date for Minoan eruption of Santorini, *Geochem. Geophys. Geosy.*, 5, Q03005, doi:10.1029/2003GC000672, 2004b.
- Pearce, N. J. G., Denton, J. S., Perkins, W. T., Westgate, J. A., and Alloway, B. V.: Correlation and characterisation of individual glass shards from tephra deposits using trace element laser ablation ICP-MS analyses: current status and future potential, *J. Quaternary Sci.*, 22, 721–236, 2007.
- Pearce, N. J. G., Perkins, W. T., Westgate, J. A., and Wade, S. C.: Trace element analysis by laser ablation ICP-MS: the quest for comprehensive chemical characterisation of single sub-10 µm volcanic glass shards, *Quatern. Int.*, 246, 57–81, 2011.
- Pilcher, J. R., Hall, V. A., and McCormac, F. G.: An outline tephrochronology for the Holocene of the north of Ireland, *J. Quaternary Sci.*, 11, 485–494, 1996.
- Ponomareva, V. V., Kyle, P. R., Melekestsev, I. V., Rinkleff, P. G., Dirksen, O. V., Sulerzhitsky, L. D., Zaretskaia, N. E., and Rourke, R.: The 7600 (<sup>14</sup>C) year BP Kurile Lake caldera-forming eruption, Kamchatka, Russia: stratigraphy and field relationships, *J. Volcanol. Geoth. Res.*, 136, 199–222, 2004.
- Ponomareva, V. V., Churikova, T. G., Melekestsev, I., Braitseva, O. A., Pevzner, M. M., and Sulerzhitsky, L. D.: Late Pleistocene–Holocene volcanism on the Kamchatka Peninsula, Northwest Pacific region, in: *Volcanism and Subduction: the Kamchatka Region*, edited by: Eichelberger, J., Izbekov, P., Ruppert, N., Lees, J., and Gordeev, E., AGU Geophysical Monograph Series, 172, 165–198, 2007.
- Ponomareva, V. V., Portnyagin, M. V., Derkachev, A. N., Pendea, I. F., Bourgeois, J., Reimer, P. J., Garbe-Schönberg, D., and Krashennnikov, S.: Early Holocene M~6 explosive eruption from Plosky volcanic massif (Kamchatka) and its tephra as a link between terrestrial and marine paleoenvironmental records, *Int. J. Earth Sci.*, 102, 1673–1699, doi:10.1007/s00531-013-0898-0, 2013a.
- Ponomareva, V. V., Portnyagin, M. V., Derkachev, A. N., Juschus, O., Garbe-Schönberg, D., and Nürnberg, D.: Identification of a widespread Kamchatkan tephra: a middle Pleistocene tie-point between Arctic and Pacific paleoclimatic records, *Geophys. Res. Lett.*, 40, 3538–3543, doi:10.1002/grl.50645, 2013b.
- Preece, S., Westgate, J., Stemper, B., and Péwé, T.: Tephrochronology of late Cenozoic loess at Fairbanks, central Alaska, *Geol. Soc. Am. Bull.*, 111, 71–90, 1999.

6014

- Preece, S. J., Westgate, J. A., Alloway, B. V., and Milner, M. W.: Characterization, identity, distribution, and source of late Cenozoic tephra beds in the Klondike district of the Yukon, Canada, *Can. J. Earth Sci.*, 37, 983–996, 2000.
- Preece, S. J., Westgate, J. A., Froese, D. G., Pearce, N. J. G., Perkins, W. T., and Fisher, T.: A catalogue of late Cenozoic tephra beds in the Klondike goldfields and adjacent areas, Yukon Territory, *Can. J. Earth Sci.*, 48, 1386–1418, doi:10.1139/e10-110, 2011a.
- Preece, S. J., Pearce, N. J. G., Westgate, J. A., Froese, D. G., Jensen, B. J. L., and Perkins, W. T.: Old Crow tephra across eastern Beringia: a single cataclysmic eruption at the close of Marine Isotope Stage 6, *Quaternary Sci. Rev.*, 30, 2069–2090, doi:10.1016/j.quascirev.2010.04.020, 2011b.
- Prueher, L. M. and Rea, D. K.: Tephrochronology of the Kamchatka–Kurile and Aleutian arcs: evidence for volcanic episodicity, *J. Volcanol. Geoth. Res.*, 106, 67–84, 2001.
- Pyne-O'Donnell, S. D. F., Hughes, P. D. M., Froese, D. G., Jensen, B. J. L., Kuehn, S. C., Mallon, G., Amesbury, M. J., Charman, D. J., Daley, T. J., Loader, N. J., Mauquoy, D., Alayne Street-Perrott, A., and Woodman-Ralph, J.: High-precision ultra-distal Holocene tephrochronology in North America, *Quaternary Sci. Rev.*, 52, 6–11, doi:10.1016/j.quascirev.2012.07.024, 2012.
- Reyes, A. V., Froese, D. G., and Jensen, B. J. L.: Permafrost response to last interglacial warming: field evidence from non-glaciated Yukon and Alaska, *Quaternary Sci. Rev.*, 29, 3256–3274, doi:10.1016/j.quascirev.2010.07.013, 2010.
- Richter, D. H., Smith, J. G., Lanphere, M. A., Dalrymple, G. B., Reed, B. L., and Shew, N.: Age and progression of volcanism, Wrangell volcanic field, Alaska, *B. Volcanol.*, 53, 29–44, 1990.
- Rosman, K. J. R. and Taylor, P. D. P.: Isotopic Composition of the Elements, International Union of Pure and Applied Chemistry, 22, 1997.
- Sauerbrey, M. A., Juschus, O., Gebhardt, A. C., Wennrich, V., Nowaczyk, N. R., and Melles, M.: Mass movement deposits in the 3.6 Ma sediment record of Lake El'gygytyn, Far East Russian Arctic, *Clim. Past*, 9, 1949–1967, doi:10.5194/cp-9-1949-2013, 2013.
- Schirmermeister, L., Froese, D., Tumskey, V., Grosse, G., and Wetterich, S.: Yedoma: Late Pleistocene ice-rich syngenetic permafrost of Beringia, *Encyclopedia Quaternary Sci.*, 3, 542–552, 2013.
- Shane, P. A. R., Black, T. M., Alloway, B. V., and Westgate, J. A.: Early to middle Pleistocene tephrochronology of North Island, New Zealand: implications for volcanism, tec-

6015

- tonism, and paleoenvironments, *Geol. Soc. Am. Bull.*, 108, 915–925, doi:10.1130/0016-7606(1996)108<0915:ETMPTO>2.3.CO;2, 1996.
- Sher, A. V.: Problems of the last interglacial in Arctic Siberia, *Quatern. Int.*, 10–12, 215–222, 1991.
- Sher, A. V.: Yedoma as a store of paleoenvironmental records in Beringia, in: *Beringia Paleoenvironmental Workshop, September 1997, Abstracts and Program*, edited by: Elias, S. and Brigham-Grette, J., 92–94, 1997.
- Siebert, L. and Simkin, T.: *Volcanoes of the World: an Illustrated Catalog of Holocene Volcanoes and their Eruptions*, Smithsonian Institution, Global Volcanism Program, Digital Information Series, GVP-3, available at: <http://www.volcano.si.edu/world/>, 2002.
- Sun, S. and McDonough, W. F.: Chemical and isotopic systematics of oceanic basalts: implications for mantle compositions and processes, in: *Magmatism in the Ocean Basins*, edited by: Sanders, A. D. and Norry, M. J., Geological Society Special Publication, 313–345, 1989.
- van den Bogaard, C. and Schmincke, H. U.: Linking the North Atlantic to Central Europe: a high-resolution Holocene tephrochronological record from Northern Germany, *J. Quaternary Sci.*, 17, 3–20, doi:10.1002/jqs.636, 2002.
- Wastegård, S.: Late Quaternary tephrochronology of Sweden: a review, *Quatern. Int.*, 130, 49–62, doi:10.1016/j.quaint.2004.04.030, 2002.
- Westgate, J., Stemper, B., and Péwé, T.: A 3 my record of Pliocene–Pleistocene loess in interior Alaska, *Geology*, 18, 858–861, 1990.
- Westgate, J., Preece, S., Froese, D., Walter, R., Sandhu, A., and Schweger, C.: Dating early and middle (Reid) Pleistocene glaciations in central Yukon by tephrochronology, *Quaternary Res.*, 56, 335–348, 2001.
- Westgate, J. A., Preece, S. J., Froese, D. G., Telka, A. M., Storer, J. E., Pearce, N. J. G., Enkin, R. J., Jackson, L. E., LeBarge, W., and Perkins, W. T.: Gold Run tephra: a Middle Pleistocene stratigraphic and paleoenvironmental marker across west-central Yukon Territory, Canada, *Can. J. Earth Sci.*, 46, 465–478, 2009.
- Westgate, J. A., Pearce, N. J. G., Perkins, W. T., Shane, P., and Preece, S. J.: Lead isotope ratios of volcanic glass by laser ablation inductively-coupled plasma mass spectrometry: application to Miocene tephra beds in Montana, USA and adjacent areas, *Quatern. Int.*, 246, 82–96, 2011a.
- Westgate, J. A., Preece, S. J., and Jackson, L. E.: Revision of the tephrostratigraphy of the lower Sixtymile River area, Yukon Territory, Canada, *Can. J. Earth Sci.*, 48, 695–701, 2011b.



6016

**Table 1.** Positions and ages of tephra layers identified in Lake El'gygytyn sediments. Core abbreviations are: 1–PG1351, 2–Lz1024, A–5011-1A, B–5011-1B, C–5011-1C. Ages and composite depth of tephra layers from Nowaczyk et al. (2013).

Tephra	Core	Lab ID Kiel	Lab ID Alberta	Depth in 1, 2 (m)	Depth in A (m)	Depth in B (m)	Composite core depth (m)	Thickness (cm)	Age estimate (ka)	Description
T0	1, 2	T 0-4 core 1	UA1936, UA1937, UA1938	2.12–2.13 in 1			2.54–2.55	1	> 45 (Anderson, Lozhkin, 2002)	yellowish
T1	1, 2, A, B	T1-2 core 2 T1-3/ ET1-3 core B	UA1939, UA1949, UA1941	7.93 in 2	5.085– 5.095	5.148– 5.158	788– 789 cm	1	177	yellowish
T2	A, B	T2-1 core A T2-2 core B	UA1942, UA1943		24.415– 24.420	24.293– 24.298	27.52– 27.52	0.5	674	greyish
T3	A, B	T3-1 core B T3-2 core B T3-3 core B	UA1944, UA1945, UA1946, UA1947		33.090– 33.159	32.971– 33.027	36.41– 36.47	6	918	Normally graded ash: fine medium to coarse sand sized ash
T4	A, B	T4-1 core A T4-4 core B	UA1948, UA1949, UA1950, UA1951		56.565– 56.576	56.989– 57.000	60.79– 60.80	5	1411	sandy white folded layer
T5	A, B	T5-1 core A T5-3 core B	UA1951, UA1953, UA1954		58.519– 58.559	58.433– 57.000	62.04– 62.08	4	1434	black layer
T6	A, B	T6-1 core A T6-2 core B	UA1955, UA1956		75.092– 75.099	75.167– 75.176	79.25– 79.26	0.7–0.9	1775	white
T7	A, B, C	T7-1 core B T7-2 core B	UA2014, UA2015			100.715– 100.785	104.93– 105.00	0.45	2225	white/grey

6017

**Table 2.** Major-element geochemistry of Lake El'gygytyn tephra from both the University of Alberta (UA) and Kiel laboratories. The combined mean and standard deviations of both UA and Kiel data sets are in bold.

Lab	Tephra	SiO <sub>2</sub>	TiO <sub>2</sub>	Al <sub>2</sub> O <sub>3</sub>	FeO	MnO	MgO	CaO	Na <sub>2</sub> O	K <sub>2</sub> O	P <sub>2</sub> O <sub>5</sub>	F	SO <sub>3</sub>	Cl	Total	
UA	T0	MEAN	72.89	0.50	14.01	2.88	0.13	0.57	2.45	4.65	1.77			0.15	100.00	
		STDEV	0.52	0.06	0.26	0.13	0.04	0.06	0.13	0.15	0.07			0.03	0.00	
		n	70	70	70	70	70	70	70	70	70			70	70	
Kiel	T0	MEAN	72.64	0.50	13.94	2.86	0.13	0.54	2.36	4.97	1.79	0.08	0.03	0.01	100.00	
		STDEV	0.72	0.04	0.34	0.14	0.04	0.08	0.21	0.09	0.07	0.02	0.03	0.01	0.01	0.00
		n	19	19	19	19	19	19	19	19	19	19	19	19	19	
Both	T0	MEAN	<b>72.84</b>	<b>0.50</b>	<b>14.00</b>	<b>2.88</b>	<b>0.13</b>	<b>0.57</b>	<b>2.43</b>	<b>4.72</b>	<b>1.78</b>	<b>0.11</b>	<b>0.03</b>	<b>0.01</b>	<b>0.15</b>	<b>100.00</b>
		STDEV	<b>0.57</b>	<b>0.05</b>	<b>0.27</b>	<b>0.13</b>	<b>0.04</b>	<b>0.06</b>	<b>0.16</b>	<b>0.19</b>	<b>0.07</b>	<b>0.03</b>	<b>0.03</b>	<b>0.01</b>	<b>0.02</b>	<b>0.00</b>
		n	<b>89</b>	<b>89</b>	<b>89</b>	<b>89</b>	<b>89</b>	<b>89</b>	<b>89</b>	<b>89</b>	<b>89</b>	<b>89</b>	<b>89</b>	<b>89</b>	<b>89</b>	
UA	T1	MEAN	77.77	0.24	12.38	1.22	0.06	0.22	1.20	3.96	2.80			0.16	100.00	
		STDEV	0.39	0.06	0.22	0.13	0.03	0.03	0.08	0.15	0.11			0.03	0.00	
		n	73	73	73	73	73	73	73	73	73			73	73	
Kiel	T1	MEAN	77.57	0.22	12.37	1.16	0.06	0.20	1.19	4.21	2.79	0.02	0.03	0.01	100.00	
		STDEV	0.17	0.02	0.10	0.10	0.04	0.02	0.03	0.12	0.08	0.02	0.04	0.01	0.01	0.00
		n	71	71	71	71	71	71	71	71	71	71	71	71	71	
Both	T1	MEAN	<b>77.67</b>	<b>0.23</b>	<b>12.37</b>	<b>1.19</b>	<b>0.06</b>	<b>0.21</b>	<b>1.20</b>	<b>4.08</b>	<b>2.80</b>	<b>0.02</b>	<b>0.03</b>	<b>0.01</b>	<b>0.16</b>	<b>100.00</b>
		STDEV	<b>0.32</b>	<b>0.05</b>	<b>0.18</b>	<b>0.12</b>	<b>0.03</b>	<b>0.03</b>	<b>0.06</b>	<b>0.19</b>	<b>0.10</b>	<b>0.02</b>	<b>0.04</b>	<b>0.01</b>	<b>0.02</b>	<b>0.00</b>
		n	<b>144</b>	<b>144</b>	<b>144</b>	<b>144</b>	<b>144</b>	<b>144</b>	<b>144</b>	<b>144</b>	<b>144</b>	<b>71</b>	<b>71</b>	<b>71</b>	<b>144</b>	
UA	T2	MEAN	74.14	0.41	13.63	2.52	0.10	0.40	1.81	4.25	2.58			0.16	100.00	
		STDEV	1.20	0.09	0.38	0.36	0.04	0.11	0.35	0.20	0.15			0.03	0.00	
		n	52.00	52.00	52.00	52.00	52.00	52.00	52.00	52.00	52.00			52.00	52.00	
Kiel	T2	MEAN	73.21	0.42	13.78	2.61	0.10	0.42	1.88	4.76	2.53	0.06	0.06	0.01	100.00	
		STDEV	0.95	0.07	0.27	0.32	0.04	0.09	0.26	0.17	0.11	0.02	0.05	0.01	0.01	0.00
		n	49	49	49	49	49	49	49	49	49	49	49	49	49	
Both	T2	MEAN	<b>73.69</b>	<b>0.41</b>	<b>13.70</b>	<b>2.56</b>	<b>0.10</b>	<b>0.41</b>	<b>1.84</b>	<b>4.50</b>	<b>2.56</b>	<b>0.06</b>	<b>0.06</b>	<b>0.01</b>	<b>0.16</b>	<b>100.00</b>
		STDEV	<b>1.17</b>	<b>0.08</b>	<b>0.34</b>	<b>0.35</b>	<b>0.04</b>	<b>0.10</b>	<b>0.31</b>	<b>0.31</b>	<b>0.13</b>	<b>0.02</b>	<b>0.05</b>	<b>0.01</b>	<b>0.02</b>	<b>0.00</b>
		n	<b>101</b>	<b>101</b>	<b>101</b>	<b>101</b>	<b>101</b>	<b>101</b>	<b>101</b>	<b>101</b>	<b>101</b>	<b>49</b>	<b>49</b>	<b>49</b>	<b>101</b>	
UA	T3	MEAN	69.71	0.75	14.57	3.99	0.15	0.94	3.07	4.62	2.05			0.13	100.00	
		STDEV	1.56	0.09	0.34	0.59	0.03	0.23	0.49	0.27	0.19			0.03	0.00	
		n	70	70	70	70	70	70	70	70	70			70	70	
Kiel	T3	MEAN	69.25	0.73	14.63	3.93	0.14	0.89	2.94	5.05	2.08	0.15	0.05	0.03	100.00	
		STDEV	1.33	0.07	0.47	0.50	0.05	0.22	0.47	0.23	0.16	0.05	0.04	0.02	0.01	0.00
		n	81	81	81	81	81	81	81	81	81	81	81	81	81	
Both	T3	MEAN	<b>69.47</b>	<b>0.74</b>	<b>14.61</b>	<b>3.96</b>	<b>0.15</b>	<b>0.91</b>	<b>3.00</b>	<b>4.85</b>	<b>2.07</b>	<b>0.15</b>	<b>0.05</b>	<b>0.03</b>	<b>0.13</b>	<b>100.00</b>
		STDEV	<b>1.46</b>	<b>0.08</b>	<b>0.41</b>	<b>0.54</b>	<b>0.04</b>	<b>0.23</b>	<b>0.48</b>	<b>0.33</b>	<b>0.17</b>	<b>0.05</b>	<b>0.04</b>	<b>0.02</b>	<b>0.02</b>	<b>0.00</b>
		n	<b>151</b>	<b>151</b>	<b>151</b>	<b>151</b>	<b>151</b>	<b>151</b>	<b>151</b>	<b>151</b>	<b>151</b>	<b>81</b>	<b>81</b>	<b>81</b>	<b>151</b>	
UA	T4	Mean	71.33	0.68	14.23	3.42	0.16	0.64	2.20	4.90	2.31			0.13	100.00	
		STDev	0.33	0.06	0.11	0.11	0.04	0.04	0.10	0.27	0.06			0.03	0.00	
		n	118	118	118	118	118	118	118	118	118			118	118	
Kiel	T4	MEAN	70.52	0.69	14.34	3.43	0.16	0.66	2.19	5.34	2.34	0.12	0.05	0.02	100.00	
		STDEV	0.23	0.02	0.12	0.20	0.04	0.03	0.06	0.12	0.04	0.02	0.05	0.01	0.01	0.00
		n	42	42	42	42	42	42	42	42	42	42	42	42	42	
Both	T4	MEAN	<b>71.00</b>	<b>0.68</b>	<b>14.29</b>	<b>3.43</b>	<b>0.16</b>	<b>0.65</b>	<b>2.21</b>	<b>5.05</b>	<b>2.32</b>	<b>0.12</b>	<b>0.05</b>	<b>0.02</b>	<b>0.13</b>	<b>100.00</b>
		STDEV	<b>0.48</b>	<b>0.05</b>	<b>0.12</b>	<b>0.15</b>	<b>0.04</b>	<b>0.03</b>	<b>0.08</b>	<b>0.35</b>	<b>0.06</b>	<b>0.02</b>	<b>0.05</b>	<b>0.01</b>	<b>0.02</b>	<b>0.00</b>
		n	<b>110</b>	<b>110</b>	<b>110</b>	<b>110</b>	<b>110</b>	<b>110</b>	<b>110</b>	<b>110</b>	<b>110</b>	<b>42</b>	<b>42</b>	<b>42</b>	<b>110</b>	

6018



**Table 3a. Continued.**

Sample number	Tephra	Eu	Gd	Tb	Dy	Ho	Er	Tm	Yb	Lu	Hf	Ta	Pb	Th	U
UA1936 avg. s.d. n = 21	T0	1.86 0.37	10.2 1.1	1.78 0.31	11.6 1.6	2.58 0.40	7.89 1.02	1.17 0.19	7.75 1.01	1.29 0.15	7.91 1.19	0.43 0.11	15.5 6.1	3.56 0.54	1.57 0.33
UA1939 avg. s.d. n = 24	T1	0.85 0.16	5.69 0.78	0.86 0.13	6.06 1.09	1.39 0.25	4.64 1.09	0.74 0.18	4.92 0.77	0.84 0.15	7.71 1.15	0.51 0.12	18.4 4.9	5.24 0.66	2.52 0.50
UA1943 avg. s.d. n = 9	T2	1.71 0.33	10.3 1.3	1.56 0.23	9.95 1.37	2.50 0.52	7.29 0.86	1.07 0.12	7.72 0.96	1.22 0.23	10.79 1.81	0.66 0.14	22.4 5.9	7.81 1.79	3.09 0.88
UA1942 avg. s.d. n = 16	T3	1.72 0.32	9.90 2.29	1.72 0.40	11.4 2.7	2.55 0.55	7.56 1.80	1.09 0.20	8.54 2.90	1.12 0.26	11.59 3.18	0.71 0.25	32.4 26.8	8.83 3.61	3.50 1.30
UA1947 avg. s.d. n = 26	T3	2.10 0.36	11.5 2.2	1.78 0.28	12.1 1.7	2.58 0.33	7.98 1.19	1.16 0.25	7.98 1.11	1.25 0.18	9.26 1.00	0.68 0.20	16.7 3.1	4.67 1.54	2.05 0.63
T3-2 avg. s.d. n = 10	T3 Kiel Mount	2.10 0.25	11.6 1.9	1.98 0.16	12.1 1.6	2.73 0.30	7.81 0.57	1.29 0.23	7.93 0.95	1.24 0.15	9.68 1.11	0.52 0.07	14.4 1.1	4.38 0.63	1.61 0.15
	<b>T3 (Overall average)</b> s.d. n = 52	<b>1.98</b> <b>0.37</b>	<b>11.0</b> <b>2.3</b>	<b>1.80</b> <b>0.31</b>	<b>11.9</b> <b>2.0</b>	<b>2.60</b> <b>0.40</b>	<b>7.82</b> <b>1.32</b>	<b>1.16</b> <b>0.24</b>	<b>8.14</b> <b>1.82</b>	<b>1.21</b> <b>0.21</b>	<b>10.06</b> <b>2.18</b>	<b>0.66</b> <b>0.21</b>	<b>21.1</b> <b>16.6</b>	<b>5.89</b> <b>3.00</b>	<b>2.41</b> <b>1.12</b>
UA1944 avg. s.d. n = 20	T4	1.93 0.55	10.6 2.9	1.80 0.50	11.9 3.7	2.64 0.77	8.19 2.45	1.24 0.39	7.55 1.90	1.22 0.40	9.89 2.76	0.56 0.23	15.1 3.8	4.96 1.25	1.78 0.46
T4-1 avg. s.d. n = 10	T4 Kiel mount	2.17 0.27	10.9 1.6	1.69 0.24	10.8 1.1	2.30 0.25	7.19 0.80	1.09 0.15	7.15 0.94	0.99 0.14	8.38 0.89	0.60 0.11	16.7 1.3	3.51 0.43	1.92 0.15
	<b>T4 (Overall average)</b> s.d. n = 30	<b>2.09</b> <b>0.35</b>	<b>11.1</b> <b>1.7</b>	<b>1.83</b> <b>0.30</b>	<b>12.3</b> <b>2.7</b>	<b>2.65</b> <b>0.50</b>	<b>8.45</b> <b>1.62</b>	<b>1.25</b> <b>0.28</b>	<b>7.79</b> <b>1.04</b>	<b>1.22</b> <b>0.32</b>	<b>10.04</b> <b>1.88</b>	<b>0.60</b> <b>0.20</b>	<b>15.9</b> <b>2.6</b>	<b>4.76</b> <b>1.16</b>	<b>1.91</b> <b>0.28</b>
UA1952 avg. s.d. n = 27	T5	1.73 0.36	7.23 1.33	1.16 0.32	7.25 1.58	1.57 0.40	4.51 1.07	0.70 0.21	4.71 1.40	0.70 0.22	4.80 1.46	0.34 0.18	10.5 2.0	1.92 0.52	1.03 0.27
UA1955 avg. s.d. n = 23	T5	1.91 0.29	6.76 1.09	0.99 0.24	6.41 1.05	1.34 0.25	3.64 0.74	0.58 0.11	4.06 0.80	0.61 0.16	4.24 1.17	0.27 0.12	6.77 0.92	1.78 0.40	0.82 0.20
	<b>T5 (Overall average)</b> s.d. n = 50	<b>1.82</b> <b>0.34</b>	<b>7.01</b> <b>1.24</b>	<b>1.08</b> <b>0.29</b>	<b>6.86</b> <b>1.41</b>	<b>1.46</b> <b>0.36</b>	<b>4.11</b> <b>1.03</b>	<b>0.65</b> <b>0.18</b>	<b>4.41</b> <b>1.19</b>	<b>0.66</b> <b>0.20</b>	<b>4.54</b> <b>1.35</b>	<b>0.31</b> <b>0.16</b>	<b>8.76</b> <b>2.43</b>	<b>1.86</b> <b>0.47</b>	<b>0.93</b> <b>0.26</b>
T6-02 avg. s.d. n = 25	T6 Kiel Mount	1.81 0.24	9.86 1.53	1.65 0.25	10.8 1.8	2.32 0.36	7.06 1.15	1.05 0.19	6.95 1.15	1.11 0.17	9.64 1.77	0.73 0.16	23.4 4.3	4.98 0.97	2.33 0.36
UA2014 avg. s.d. n = 15	T7	0.71 0.20	4.43 0.73	0.75 0.14	4.53 0.84	1.06 0.14	3.17 0.52	0.50 0.11	3.73 0.64	0.62 0.21	5.29 0.75	0.69 0.11	22.9 3.3	10.9 1.0	4.16 0.36

**Table 3a. Continued.**

Sample number	Tephra	Crater diameter μm	Int'l std -- SiO <sub>2</sub> , wt%	Avg CaO (43 + 44) wt%	Rb	Sr	Y	Zr	Nb	Cs	Ba	La	Ce	Pr	Nd	Sm
<i>Reference Material Analyses</i>																
ATHO-G, This study, 20 μm analyses sd (n = 10)					63.5	93.9	95.4	506	62.6	1.01	537	54.2	122	14.5	62.8	13.9
ATHO-G Reference conc. GeoReM s.d					2.2	4.2	6.7	27	2.20	0.11	14	2.3	3	0.4	3.2	0.9
					<b>65.3</b>	<b>94.1</b>	<b>94.5</b>	<b>512</b>	<b>62.4</b>	<b>1.08</b>	<b>547</b>	<b>55.6</b>	<b>121</b>	<b>14.6</b>	<b>60.9</b>	<b>14.2</b>
					<b>3</b>	<b>2.7</b>	<b>3.5</b>	<b>20</b>	<b>2.6</b>	<b>0.11</b>	<b>16</b>	<b>1.5</b>	<b>4</b>	<b>0.4</b>	<b>2</b>	<b>0.4</b>
<i>Selected data for widespread Alaskan Tephra</i>																
Aniakchak 1643 BC		LA-ICP-MS			71.4	251.29	44.9	227	13.0	n.d.	724.9	30.9	57.0	8.25	35.3	8.61
Aniakchak 1643 BC		Solution ICP-MS			66.5	199	46.3	267	15.5	3.11	861	26.4	57.4	6.96	30.6	7.66
UT-1		Solution ICP-MS			103	138	34.7	259	n.d.	4.37	923	24.7	52.8	5.83	23.7	5.57
UT613		Solution ICP-MS	Old Crow Tephra		99.3	151.07	29.9	233	8.95	4.47	1003	26.2	46.4	6.66	25.5	5.50
Dawson Tephra		Solution ICP-MS	Old Crow Tephra		85.0	73.23	39.6	299	7.31	5.13	920	19.7	40.6	5.86	23.4	5.82



**Table 3a.** Continued.

Sample number	Tephra	Eu	Gd	Tb	Dy	Ho	Er	Tm	Yb	Lu	Hf	Ta	Pb	Th	U
<i>Reference Material Analyses</i>															
ATHO-G, This study, 20 µm analyses		2.69	15.7	2.46	16.5	3.47	10.3	1.54	10.2	1.58	13.5	3.87	5.54	7.51	2.41
sd (n = 10)		0.3	1.4	0.13	1.1	0.32	0.8	0.14	0.7	0.15	0.9	0.20	0.55	0.40	0.14
ATHO-G Reference conc, GeoReM		2.76	15.3	2.51	16.2	3.43	10.3	1.52	10.5	1.54	13.7	3.9	5.67	7.4	2.37
s.d		0.1	0.7	0.08	0.7	0.11	0.5	0.07	0.4	0.05	0.5	0.2	0.62	0.27	0.12
<i>Selected data for widespread Alaskan Tephra</i>															
Aniakchak 1643 BC		2.30	9.29	1.45	8.95	1.91	5.04	0.78	5.55	0.85	6.07	0.70	13.2	9.01	2.56
Aniakchak 1643 BC		1.71	6.54	1.27	7.74	1.82	4.84	0.73	4.78	0.74	n.d.	1.03	n.d.	6.13	2.84
UT-1 Old Crow Tephra		0.87	4.83	0.90	5.34	1.27	3.44	0.56	3.60	0.57	7.00	n.d.	n.d.	9.81	4.28
UT613 Old Crow Tephra		1.07	5.83	0.94	5.47	1.20	3.49	0.55	3.84	0.62	7.46	0.76	13.3	10.2	5.13
Dawson Tephra		0.95	6.33	1.07	6.76	1.46	4.31	0.76	4.64	0.80	8.43	0.50	n.d.	7.50	4.02

6023

**Table 3b.** Average trace-element composition of single glass shards from Lake El'gytgyn tephra obtained by LA-ICP-MS in Kiel. All concentrations are in ppm unless otherwise stated.

Sample number	Tephra	Crater diameter, µm	Int'l std - CaO, wt%	Li	SiO <sub>2</sub> wt%	Sc	Ti	V	Cu	Zn	Ga	As	Rb	Sr	Y	Zr	Nb	Mo	Sb	Cs
T0-4	T0	Average s.d. n = 7	All 50 µm 2.35	25.2 2.5	66.2 5.2	18.6 1.1	2817 120	9.20 1.30	7.17 0.70	65.3 14.1	16.3 1.5	6.83 1.41	37.1 4.1	145 2	42.6 3.8	160 17	2.94 0.32	1.52 0.22	0.47 0.08	2.01 0.29
T1-2	T1	Average s.d. n = 6	All 50 µm 1.19	24.1 1.9	72.5 3.4	6.36 0.27	1407 76	11.2 3.3	8.06 1.02	38.7 6.4	13.3 0.7	8.58 1.05	52.0 1.4	113 9	21.8 0.8	155 6	3.23 0.18	2.79 0.26	0.62 0.09	2.34 0.13
T2-1	T2	Average s.d. n = 4	All 50 µm 1.88	30.4 2.8	65.2 4.6	12.3 0.2	2610 115	9.68 2.11	9.89 2.61	63.4 15.7	16.4 1.4	8.02 1.28	57.9 6.9	127 6	40.3 3.2	217 22	4.40 0.40	1.81 0.20	0.52 0.08	2.88 0.26
T3-3	T3	Average s.d. n = 4	All 50 µm 2.83	23.6 2.3	60.9 2.7	17.3 0.8	4433 234	32.1 6.4	11.9 3.2	66.4 10.8	17.8 0.6	8.53 2.61	41.8 3.7	184 19	42.7 3.6	211 15	4.25 0.30	1.42 0.09	0.56 0.08	2.16 0.17
T4-4	T4	Average s.d. n = 6	All 50 µm 2.17	20.3 1.4	69.6 5.1	16.1 0.4	4146 213	7.81 0.57	9.60 1.87	79.0 8.4	18.3 0.9	8.53 0.90	39.2 1.8	208 1	43.2 0.8	206 7	5.38 0.18	2.00 0.23	0.69 0.12	1.79 0.14
ET5-3	T5	Average s.d. n = 7	All 50 µm 5.96	13.5 1.7	64.1 3.3	28.2 5.2	7646 1107	135 63	16.1 9.6	110 23	20.0 1.2	6.49 3.46	24.4 9.3	382 76	32.7 6.8	130 42	3.55 1.14	1.39 0.45	0.37 0.14	1.07 0.37
ET6-2	T6	Average s.d. n = 6	All 50 µm 2.59	28.1 2.5	72.1 3.0	17.5 1.0	4366 282	11.8 1.7	14.7 3.5	258 303	17.4 0.4	14.23 7.99	49.8 1.9	184 10	43.6 2.1	253 12	7.49 0.23	2.54 0.13	1.10 0.13	2.31 0.09
T7-2	T7	Average s.d. n = 5	All 50 µm 0.58	21.4 4.1	72.0 6.2	2.65 0.19	739 50	4.98 2.23	5.78 0.46	24.6 6.8	12.4 0.6	13.80 2.06	87.8 4.9	53 2	15.8 1.0	71 6	4.46 0.33	2.99 0.30	0.91 0.11	4.25 0.36

6024

**Table 3b. Continued.**

Sample number	Tephra	Ba	La	Ce	Pr	Nd	Sm	Eu	Gd	Tb	Dy	Ho	Er	Tm	Yb	Lu	Hf	Ta	W	Pb	Th	U
T0-4	T0	438 50	10.1 0.9	24.9 2.6	3.63 0.33	17.4 1.8	5.15 0.57	1.30 0.08	5.92 0.40	1.04 0.08	7.00 0.74	1.54 0.17	4.36 0.46	0.68 0.08	4.84 0.46	0.73 0.07	4.47 0.51	0.18 0.03	0.32 0.05	7.62 0.79	1.99 0.19	0.98 0.10
T1-2	T1	679 11	12.3 0.4	26.9 0.4	3.32 0.09	13.3 0.6	3.05 0.20	0.65 0.02	3.05 0.14	0.51 0.03	3.57 0.17	0.78 0.03	2.24 0.13	0.38 0.02	2.83 0.12	0.43 0.02	4.36 0.25	0.26 0.03	0.43 0.05	11.20 0.46	3.10 0.09	1.78 0.10
T2-1	T2	718 42	14.8 1.2	34.7 3.2	4.81 0.34	21.6 1.8	5.58 0.60	1.20 0.10	5.78 0.52	0.98 0.06	6.56 0.58	1.39 0.11	4.07 0.28	0.64 0.04	4.54 0.18	0.66 0.06	5.74 0.41	0.28 0.02	0.53 0.09	9.84 1.13	3.27 0.35	1.45 0.23
T3-3	T3	561 45	13.1 1.1	31.6 2.9	4.60 0.38	21.9 1.9	5.70 0.56	1.40 0.09	6.28 0.46	1.03 0.08	6.79 0.62	1.42 0.13	4.11 0.35	0.67 0.06	4.67 0.45	0.68 0.03	5.14 0.32	0.24 0.01	0.43 0.02	7.11 0.42	2.36 0.13	1.01 0.05
T4-4	T4	649 41	15.2 0.8	35.5 1.9	5.06 0.26	23.7 1.2	6.30 0.34	1.48 0.07	6.23 0.36	1.03 0.03	6.92 0.19	1.46 0.05	4.37 0.13	0.66 0.03	4.58 0.09	0.72 0.03	5.18 0.21	0.34 0.04	0.35 0.11	10.16 0.92	2.37 0.42	1.37 0.16
ET5-3	T5	429 115	11.0 2.9	27.4 6.9	4.08 0.97	20.0 4.5	5.09 1.01	1.61 0.24	5.81 1.04	0.92 0.19	5.68 1.00	1.20 0.23	3.41 0.67	0.50 0.10	3.50 0.77	0.52 0.12	3.48 1.09	0.23 0.06	0.48 0.23	6.20 1.87	1.42 0.45	0.84 0.25
ET6-2	T6	615 23	17.1 0.6	39.6 1.9	5.43 0.31	24.8 0.9	6.32 0.35	1.47 0.03	6.61 0.40	1.08 0.10	7.27 0.40	1.57 0.06	4.61 0.21	0.70 0.05	4.71 0.25	0.74 0.04	6.56 0.18	0.50 0.03	0.69 0.14	13.40 2.25	3.44 0.14	1.67 0.03
T7-2	T7	699 48	16.0 0.9	33.7 2.6	4.02 0.29	14.9 0.7	2.80 0.20	0.45 0.05	2.35 0.26	0.36 0.04	2.29 0.10	0.53 0.04	1.51 0.13	0.25 0.03	1.86 0.19	0.26 0.03	2.50 0.28	0.33 0.03	0.97 0.20	12.42 1.03	5.84 0.50	2.53 0.27

**Table 4. Average Pb isotopic values collected on single glass shards from Lake El'gyygtyn tephra. Avg = average, sd = standard deviation.**

Samples	<sup>208</sup> Pb avg cps	Avg Pb ppm	206/204 avg	207/204 avg	208/204 avg	206/208 avg	207/208 avg	206/204 sd	207/204 sd	208/204 sd	206/208 sd	207/208 sd
T0, 30 µm	25941	15.5	19.063	16.026	39.518	0.4826	0.4055	0.870	0.846	2.024	0.0071	0.0071
RSD%, n = 19								4.6%	5.3%	5.1%	1.5%	1.8%
T1, 20 µm	16757	18.4	18.750	15.760	38.683	0.4847	0.4075	1.570	1.275	3.252	0.0065	0.0056
RSD%, n = 15								8.4%	8.1%	8.4%	1.3%	1.4%
T2, 20 µm	19016	22.4	18.951	16.090	39.299	0.4822	0.4093	1.495	1.303	2.905	0.0089	0.0091
RSD%, n = 19								7.9%	8.1%	7.4%	1.8%	2.2%
T3, 30 µm	25596	21.1	18.281	15.451	37.877	0.4825	0.4080	1.317	1.029	2.550	0.0067	0.0052
RSD%, n = 20								7.2%	6.7%	6.7%	1.4%	1.3%
ET3, 30 µm	44817	21.1	18.472	15.679	38.436	0.4806	0.4079	0.617	0.554	1.260	0.0045	0.0044
RSD%, n = 20								3.3%	3.5%	3.3%	0.9%	1.1%
T4, 20 µm	20107	15.9	18.116	15.236	37.553	0.4824	0.4059	1.172	0.899	2.426	0.0063	0.0058
RSD%, n = 17								6.5%	5.9%	6.5%	1.3%	1.4%
T5, most 30 µm, some 20 µm	24498	8.76	19.193	16.107	39.548	0.4853	0.4073	1.022	0.773	1.961	0.0072	0.0026
RSD%, n = 15								5.3%	4.8%	5.0%	1.5%	0.6%
T6, most 20 µm, some 30 µm	59358	23.4	19.090	15.752	38.884	0.4909	0.4052	1.216	0.877	2.211	0.0126	0.0056
RSD%, n = 19								6.4%	5.6%	5.7%	2.6%	1.4%
T7, 20 µm	26639	22.9	18.133	15.286	37.376	0.4854	0.4090	0.867	0.957	2.016	0.0116	0.0145
RSD%, n = 19								4.8%	6.3%	5.4%	2.4%	3.5%
Aniakchak UT2011, 20 µm	18554	12.0	19.012	15.646	38.545	0.4933	0.4060	1.368	1.106	2.770	0.0081	0.0077
RSD%, n = 18								7.2%	7.1%	7.2%	1.6%	1.9%
<b>Reference Material Analyses</b>												
GeoReM BCR-2G avg (95% CL)			<b>18.819</b>	<b>15.692</b>	<b>38.699</b>	<b>0.4863</b>	<b>0.4054</b>	<b>0.807</b>	<b>0.006</b>	<b>0.02</b>	<b>0.0005</b>	<b>0.0005</b>
BCR-2G This study 30 µm	27293	11 ± 1	18.739	15.571	38.783	0.4832	0.4015	0.830	0.707	1.771	0.0027	0.0051
RSD%, n = 10								4.4%	4.5%	4.6%	0.6%	1.3%
Accuracy This study/GeoReM			0.42%	0.77%	-0.22%	0.63%	0.95%					
GeoReM TB1-G (avg n = 2)			<b>18.333</b>	<b>15.552</b>	<b>38.611</b>	<b>0.4748</b>	<b>0.4028</b>	<b>0.001</b>	<b>0.001</b>	<b>0.004</b>		
TB-1G This study 30 µm	78931	18.4 ± 1.6	18.374	15.640	38.681	0.4750	0.4043	0.287	0.295	0.572	0.0034	0.0034
RSD%, n = 10								1.6%	1.9%	1.5%	0.7%	0.8%
Accuracy This study/GeoReM			-0.23%	-0.57%	-0.18%	-0.05%	-0.38%					

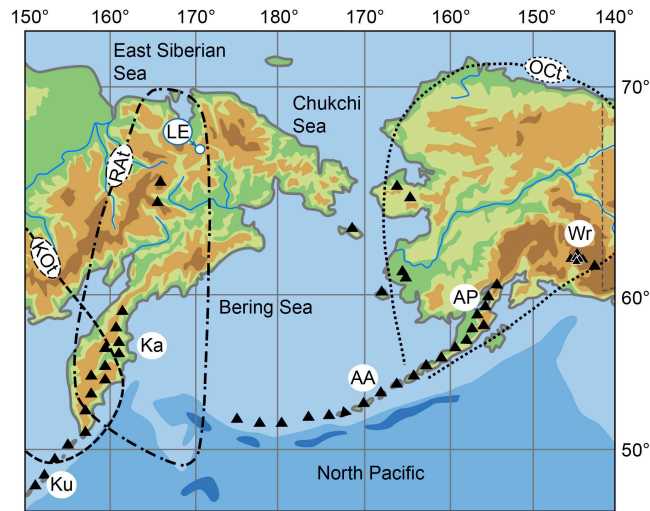


**Fig. 1.** Location of Lake El'gygytyn (LE) in relation to volcanic areas in the Kuriles (Ku), Kamchatka (Ka), Aleutian Arc (AA) and Alaska Peninsula (AP). Reconstructed distribution patterns of Old Crow Tephra (OCt; ~ 124 ka; Preece et al., 2011), Raucha Tephra (RAc; ~ 177 ka; Ponomareva et al., 2013b) and KO Tephra (KOt; ~ 7 ka; Derkachev et al., 2004) illustrate the potential for widespread tephra distribution in this region. The Wrangell volcanic field (Wr) and other smaller cinder cones and maars, indicated by additional markers, are either too far afield and/or do not produce the type of tephra deposits that are found in Lake El'gygytyn. During glacial times, the Bering shelf between Russia and Alaska was exposed, and only mountainous areas in this region experienced limited glaciation, creating the glacial refugium known as Beringia. As a result, Beringia contains terrestrial paleoenvironmental records that rival marine deposits in their richness and length.


6027

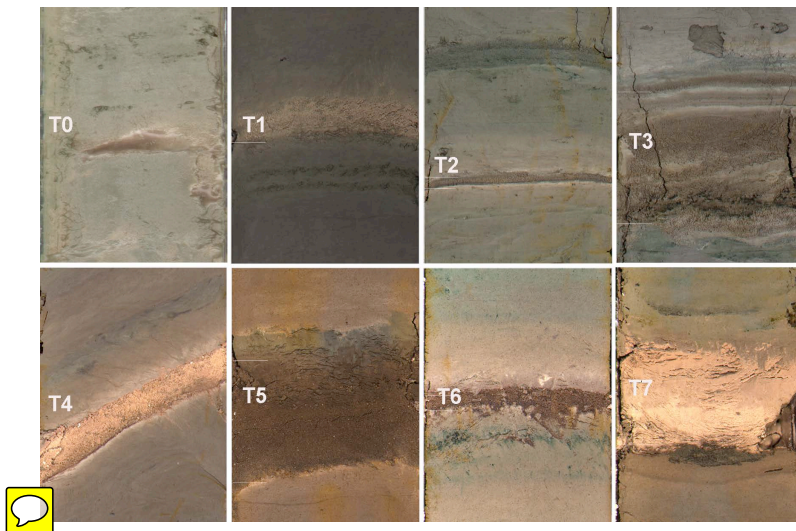


**Fig. 2.** Photos of the sections of cores with the detected tephra layers from Lake El'gygytyn: T0 (5011-4D-2H1), T1 (5011-1B-1H2), T2 (5011-1B-7H2), T3 (5011-1B-10H2), T4 (5011-1A-19H1), T5 (5011-1A-19H2), T6 (5011-1A-25H1), T7 (5011-1A-35E1). Length of each segment is 12 cm.

6028

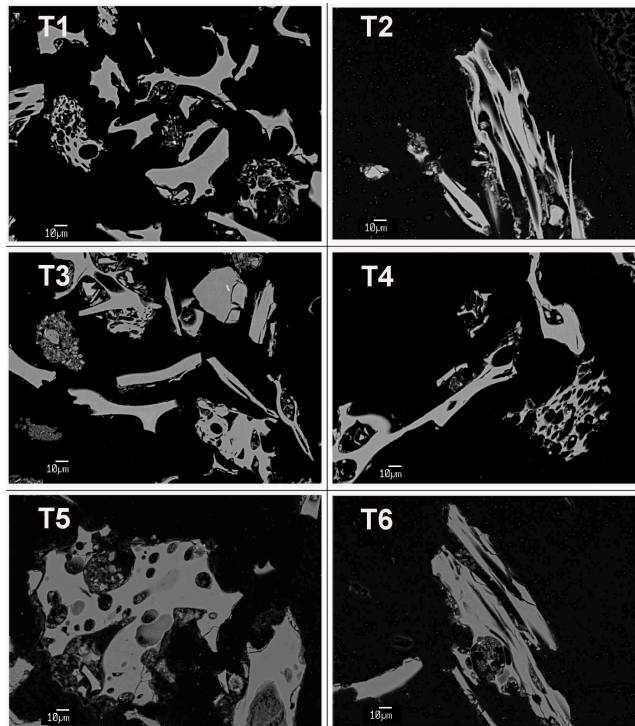


**Fig. 3.** Backscatter electron images of characteristic glass shards from tephra layers T1–T6 from Lake El'gygytyn. 

6029

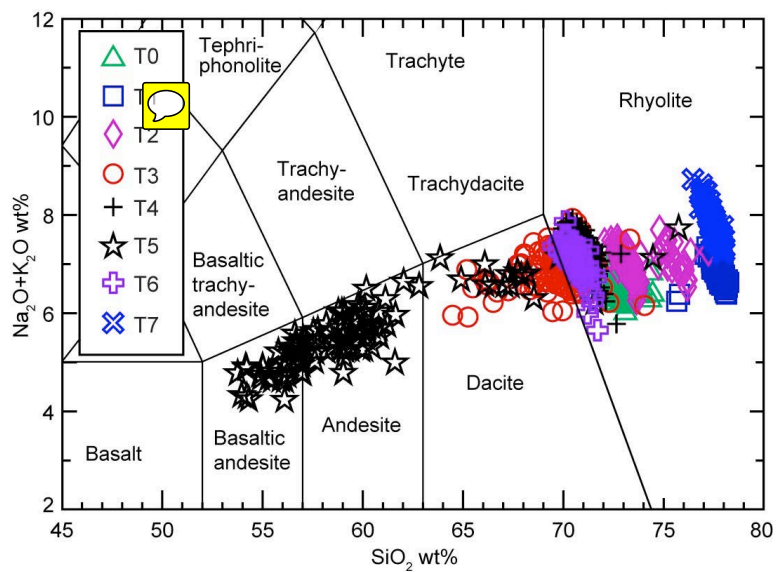


**Fig. 4.** TAS classification diagram with fields according to Le Bas et al. (1986). All data are single shard glass analyses normalized to 100 %. Data include both sets analyzed in Edmonton and Kiel.

6030

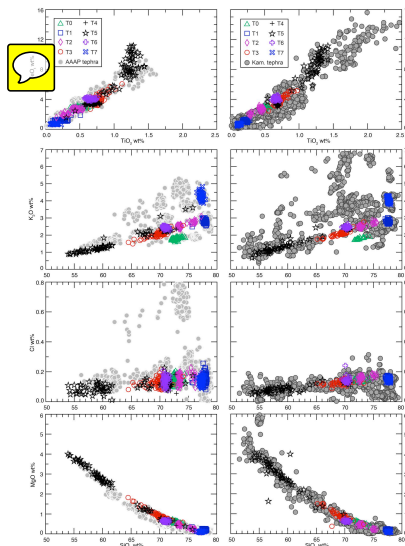


**Fig. 5.** Harker diagrams for major-element geochemistry of T0–T7 in comparison to tephra from Kamchatka and the AAAP. All data are single shard glass analyses normalized to 100%. Plots on the left compare data collected in Edmonton to a dataset of AAAP tephra that have higher similarity coefficients (> 0.90) to the tephra examined in this study. Compiled AAAP data were analyzed in Edmonton and are from the internal database, but are limited to tephra that have previously been reported in the literature. Plots on the right compare the major-element geochemical analyses collected in the Kiel laboratory in comparison to Pleistocene Kamchatkan eruptions. Although T0–T7 all plot within the fields designated by the AAAP and Kamchatkan data, they tend to plot more clearly with Kamchatkan data. This is particularly the case for the mafic oxides (e.g. MgO).

6031

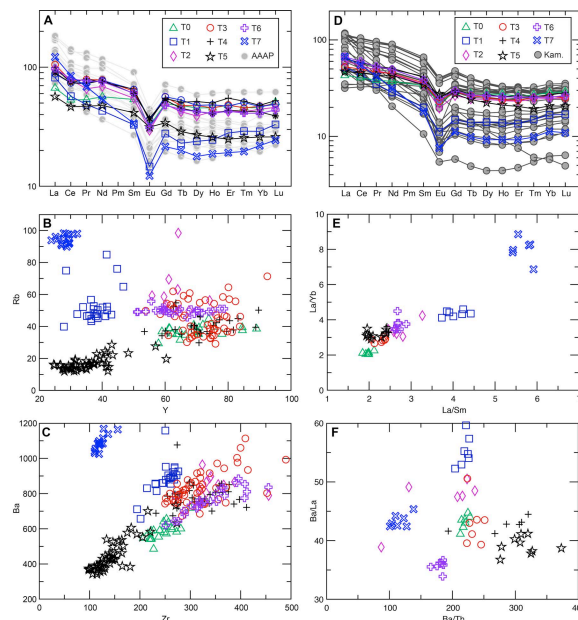


**Fig. 6.** Plots of trace-element composition of single glass shards for T0–T7, collected by LA-ICP-MS. **(A–C)** All data collected in Aberystwyth; **(D–F)** all data collected in Kiel. **(A, D)** Spider diagrams comparing the average REE abundances of each tephra to known Alaskan and Kamchatkan Pleistocene tephra (Pearce et al., 2004b; Preece et al., 2011a, b; Jensen et al., unpublished data; Portnyagin et al., unpublished data). Data are normalized to chondrite after Sun and McDonough (1989). **(B, C, E, F)** Plots of trace-elements and ratios that allow differentiation between each tephra; T1, T5, T7 are unique, but T2, T3 and T4 are very similar, with only subtle differences best portrayed in **(B)** and **(F)**.

6032



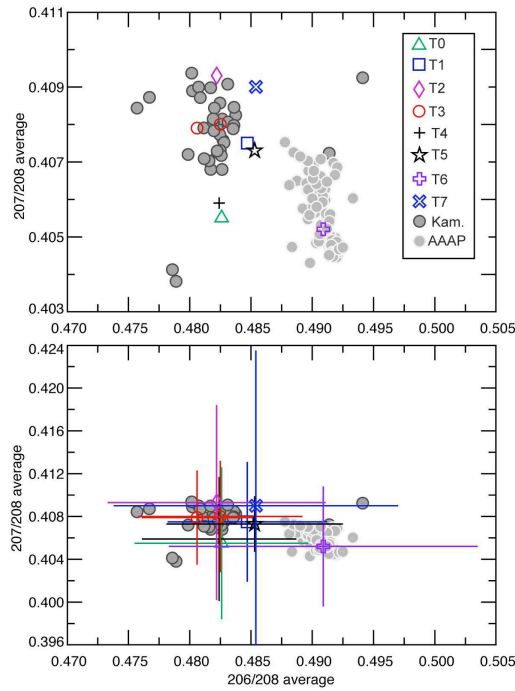


**Fig. 7.** Lead isotope composition of El'gygytyn tephra layers (T0–T7). Top: average  $^{206}\text{Pb}/^{208}\text{Pb}$  vs.  $^{207}\text{Pb}/^{208}\text{Pb}$  for samples from El'gygytyn core. Bottom: average  $^{206}\text{Pb}/^{208}\text{Pb}$  vs.  $^{207}\text{Pb}/^{208}\text{Pb}$  for samples from El'gygytyn core including  $2\sigma$  error bars. Data are plotted with previously published Pb isotope compositions of volcanic rocks from Alaska and Kamchatka (Kepezhinskias et al., 1997; Myers and Marsh, 1987; Bindeman et al., 2004; George et al., 2004; Jicha et al., 2004).

6033

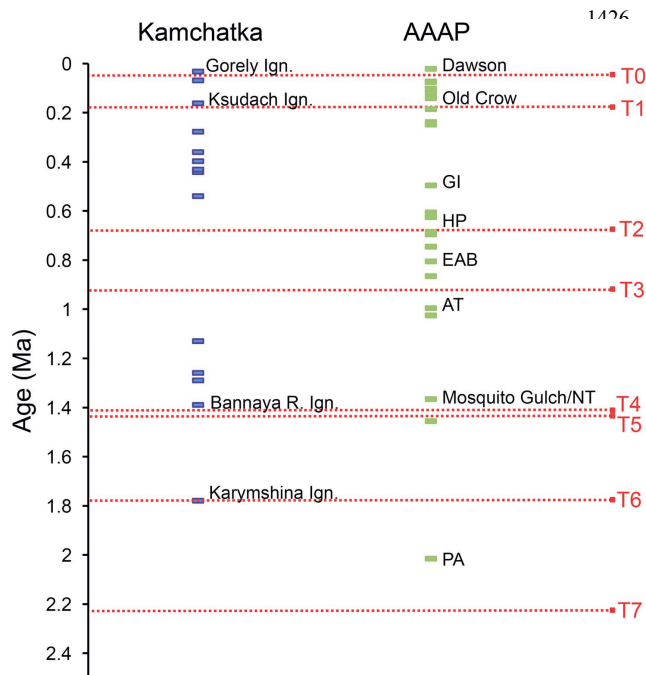


**Fig. 8.** Lake El'gygytyn tephra ages compared to ages of dated caldera eruptions in Kamchatka and ages of published distal tephra from Alaska and Yukon (after Bindemann et al., 2010; Preece et al., 1999; 2011a, b; Westgate et al., 2001, 2011b; Demuro et al., 2008). It is important to note that the frequency of eruptions in Alaska is much greater, but we limited the tephra included in this plot to ones that have been directly dated.

6034